Title	Functional expression of the P2X7 ATP receptor requires Eros
Author(s)	領田, 優太
Citation	大阪大学, 2020, 博士論文
Version Type	VoR
URL	https://doi.org/10.18910/76635
rights	
Note	

Functional expression of the P2X7 ATP receptor requires Eros

(ATP 受容体 P2X7 の機能的な発現には Eros が必要である)

大阪大学大学院生命機能研究科

免疫学フロンティア研究センター 免疫・生化学

領田優太

2020 年 3 月　博士学位論文

論文内容の要旨

Functional expression of the P2X7 ATP receptor requires Eros
（ATP 受容体 P2X7 の機能的な発現には Eros が必要である）

学位申請者　　領田　優太

P2X7 は 2 個の膜貫通領域を持つ分子量約 68,000 のタンパク質であり、細胞膜に三量体として存在する。P2X7 の細胞外領域に死細胞などから放出された ATP が結合すると、この分子は Na^+，K^+，Ca^{2+} 等の無機カチオン及び分子量 500 以下の有機カチオンを非特異的に透過させるとともに、その下流でインフラマソームを活性化、IL-1βの放出を誘導する。一方、P2X7 が活性化されると、細胞膜でリン脂質のスクランブリングが起こり、細胞表面にホスファチジルセリン（Phosphatidylserine，PS）が露出される。このように P2X7 は多彩な機能を持つタンパク質であるにも関わらず、その発現機構、作用機構及び生理作用は不明な点が多い。

今回、この ATP 刺激による P2X7 依存的な PS 露出に必要な遺伝子群を同定することを目的としてゲノムワイドな CRISPR sgRNA スクリーニングを実施した。その結果、2 個の膜貫通領域を持つ Eros （Essential for Reactive Oxygen Species）と呼ばれる膜タンパク質遺伝子が同定された。Eros をノックアウトしたマウス T 細胞株 WR19L では、野生型細胞にてみられる ATP 刺激による PS 露出が著しく減弱した。

Eros 遺伝子をノックアウトした細胞では、ATP 刺激による細胞内カルシウム濃度上昇及び有機カチオン YO-PRO-1 の取り込みも著しく減弱していた。さらにヒトマクロファージ細胞株 THP-1 やマウス骨髄由来マクロファージ（BMDM）を LPS で処理した後、ATP で刺激すると IL-1βが放出されるが、この過程も Eros 遺伝子の欠損により顕著に減少した。

Eros 遺伝子を欠損する WR19L 細胞、THP-1 細胞、BMDM では P2X7 タンパク質の発現量が大幅に減少していた。2017 年、Eros は、ER において NADPH oxidase のサブユニットに対するシャペロンとして機能することが報告されたが、同様に、Eros は ER にて P2X7 と一時的に相互作用してその発現を安定化させることを見出した。

以上、今回、Eros は NAPDH oxidase だけでなく P2X7 に対してもシャペロンとして機能し、自然免疫反応において多面的に作用することが明らかとなった。

Contents

1. Introduction

Cellular membranes are composed of a lipid bilayer (exoplasmic outer leaflet and cytoplasmic inner leaflet) with three types of lipids. The first type of lipids is glycerophospholipids [phosphatidylserine (PtdSer), phosphatidylcholine (PtdCho), phosphatidylethanolamine (PtdEtn), phosphatidylinositol (PtdIns) and phosphatidic acid (PA)]. The second one is sphingolipids, the majority of which are sphingomyelin (SM) and glycosphingolipids such as gangliosides. The third one is sterols, and cholesterol is the predominant sterol in mammalian cells (1).

Several phospholipids are asymmetrically distributed between outer and inner leaflets in the plasma membrane of eukaryotes. The outer leaflet is rich with PtdCho and SM, while PtdSer and PtdEtn are confined to the inner leaflet (1-3). The asymmetrical distribution of PtdSer and PtdEtn in the plasma membrane is mediated by a membrane protein called "flippase" that specifically translocates PtdSer and PtdEtn from the outer to inner leaflet in an ATP-dependent manner (3). Segawa et al. (4, 5) previously showed that ATP11A and ATP11C, members of P4-ATPase family, are expressed at the plasma membrane ubiquitously in various cells, and are responsible for maintaining PtdSer and PtdEtn at the inner leaflet. Like most of P4-ATPase family members, CDC50A serves as a chaperone to localize ATP11A and ATP11C to the plasma membranes, and functions as their partner for the flippase activity (4, 6).

When cells undergo apoptosis or platelets are activated, the asymmetrical distribution of phospholipids at the plasma membranes is disrupted, and the PtdSer exposed on cell surface works as an "eat me" signal of apoptotic cells, or serves on platelets as a scaffold for blood clotting factors. Caspases activated in the apoptotic cells cleave ATP11A and ATP11C to irreversibly inactivate their flippase activity, while a high concentration of Ca^{2+} evoked in activated platelets reversibly inactivates them (5). However, the inactivation of the flippases alone is not sufficient to quickly expose PtdSer in apoptotic cells (within hours) or activated platelets (within minutes), because once the asymmetrical distribution of phospholipids is established, it is not easy to spontaneously destroy it (7, 8). Thus, scramblases that nonspecifically scramble phospholipids between the outer and inner leaflets at plasma membranes have been proposed (3). Previously, Suzuki et al (9-12) identified two families of proteins, XK-related (XKR) and transmembrane protein 16 (TMEM16), each carrying 10 putative transmembrane regions as scramblases. Among 9 XKR family members, XKR4, XKR8, and XKR9 can function as a caspase-activated scramblase at plasma membranes. XKR4 and XKR9 are specifically expressed in the brain and intestines, respectively (12). On the other hand, XKR8 is ubiquitously expressed in various cells as a complex with Basigin or Neuroplastin (13), and is activated by caspase-mediated cleavage, causing the quick PtdSer-exposure in apoptotic cells. Since the flippases are inactivated by caspases, the PtdSer exposed on the cell surface of the dying cells cannot return to the inner leaflets, and works as an "eat me" signal for the engulfment by phagocytes.

Inefficient clearance of apoptotic cells is supposed to cause SLE-type autoimmune diseases (14). Accordingly, Kawano et al. found that Xkr8-deficient female mice develop SLE-type diseases in a pro-autoimmune mouse strain (15).

TMEM16F, also called anoctamin 6, belongs to the TMEM16 family, is ubiquitously expressed, and functions as a Ca^{2+}-dependent scramblase (9). Loss-of-function mutations in TMEM16F cause a delay of PtdSer-exposure and microparticle-release in human and mouse platelets, leading to prolonged bleeding time (16, 17). This observation indicates that TMEM16F is responsible for scrambling phospholipids in activated platelets in which the concentration of Ca^{2+} at the inner surface of the plasma membrane can reaches to more than 100 μM (18-20). Among other 9 TMEM16 members, TMEM16C, TMEM16D, TMEM16G and TMEM16J are present at plasma membranes and function as Ca^{2+}-dependent scramblase, but their physiological function remains unknown (11).

There are many biological processes in which scrambling of phospholipids takes place. These processes include sperm capacitation (21), lymphocyte activation (22-24) and mast cell degranulation (25). Transformed cancerous cells also reversibly expose PtdSer (26). In addition, Courageot et al. previously reported that when cells are exposed to a high concentration of extracellular ATP, they expose PtdSer (27). ATP is usually kept inside cells, and used as an energy for synthesis of macromolecules (DNA, RNA, protein and lipids) (28-32), and as a substrate for phosphorylation reactions for cell metabolism or signal transduction (33-35). Accordingly, the extracellular ATP concentration in healthy mammalian tissues is at a nanomolar range. But its concentration reaches several hundred micromolar in inflammatory sites (36-38), probably because a large amount of ATP is released from injured cells in the inflamed location (39).

Protozoa or invertebrate cells respond to the extracellular ATP, to activate the ion channels (40). Similarly, vertebrate cells respond to extracellular ATP via specific G protein-coupled receptors (P2Y receptors) and ligand-gated ion channels (P2X receptors). The P2Y receptor family consists of eight members, P2Y1, P2Y2, P2Y4, P2Y6, P2Y11, P2Y12, P2Y13 and P2Y14 (41). Members of this family bind to nucleotides including ATP, and are expressed in a tissue or cell-specific manner. They play various physiological roles such as the ion transport in epithelial cells, the chemotactic responses of neutrophils, eosinophils, macrophages and dendritic cells, and the activation and maturation of dendritic cells (42-45). P2X receptor family is comprised of seven members, P2X1, P2X2, P2X3, P2X4, P2X5, P2X6 and P2X7 (46). P2X receptors carry two transmembrane regions, and form a homo- or hetero-trimer (47, 48). They rather specifically bind to ATP, which leads to opening of a channel that non-specifically pass inorganic cations such as Na^+, K^+ and Ca^{2+} (49). While many of the P2X receptors are reported to function in neurons by modulating synaptic efficacy and sensing afferent signals from the periphery, the physiological functions of P2X receptors in other tissues or cells are less studied, except for P2X7 that plays a role in macrophages

for production of inflammatory cytokines. (50-52).

P2X7, also called P2RX7, P2X7R, or P2Z, is a unique member in the P2X family. It possesses an extra cytoplasmic C-terminal tail with more than 200 amino acids, exclusively forms a homo-trimer, and mediates a variety of events (53). Upon binding of ATP or its agonist 2'(3')-O-(4-benzoylbenzoyl)ATP (BzATP) to P2X7, rapid uptake of Na^+ and Ca^{2+}, coupled by rapid K^+-efflux, takes place without obvious desensitization (54). The K^+-mobilization is believed to ignite the NLRP3 inflammasome formation for IL-1β production in endotoxin-primed macrophages (55). The activation of P2X7 also causes the influx of small organic cations such as ethidium, N-methyl-D-glucamine (NMDG) and YO-PRO-1, although its physiological meaning is unclear (56, 57). In addition, within several minutes after the P2X7 activation, PtdSer is exposed to the cell surface, which is followed by the membrane-blebbing and micro-vesicle-release (58, 59). If the strong activation of P2X7 by ATP lasted for several minutes, cells die with the ruptured plasma membranes (60, 61). In macrophages, P2X7-dependent PtdSer exposure and the release of microvesicles are proposed to be involved in IL-1β release, in which the cleaved mature IL-1β is encapsulated in released vesicles (59). Another group showed that the released microvesicles contain TNFα converting enzyme (TACE, also called ADAM17) that cleaves membrane-bound TNFα to shed its ectodomain as a soluble cytokine (62). Thus, the secretion of cytokines (IL-1β and TNFα) is reduced in P2X7-deficeint mice (62, 63), increasing their susceptibility to infection (64). In contrast, the P2X7-deficiency ameliorates the disease phenotypes in glomerulonephritis, dermatitis and cystitis (65-67).

How a single P2X7 protein mediates these various biological processes has been elusive. In particular how PtdSer is exposed by P2X7 is not well understood, although a German group proposed an involvement of TMEM16F scramblase in this process with inadequate experimental evidence (68). For this reason, I decided to focus on the P2X7-mediated PtdSer exposure after the extracellular ATP stimulation. In this study, I found that mouse T cell line WR19L expressed P2X7, and responded strongly to ATP by exposing PtdSer in a P2X7-dependent manner. In contrast to the proposal by Ousingsawat et al. (68), the *TMEM16F* deficiency had no effect on the ATP-induced PtdSer exposure in WR19L cells. Screening of a CRISPR/Cas9 knockout library identified a molecule called "essential for reactive oxygen species (Eros)" or "cytochrome B-245 chaperone 1 (CYBC1)" as an essential factor for the P2X7-dependent PtdSer exposure. Eros was required for the expression of P2X7 not only in WR19L T cell line, but also in mouse bone marrow-derived macrophages. Accordingly, the ATP-induced Ca^{2+} uptake, organic cation influx, and IL-1β production was severely impaired in P2X7-null cells. Eros was localized to the endoplasmic reticulum and appeared to function as a chaperone for P2X7 by facilitating the formation of its homo-trimeric complex.

2. Materials and Methods

2.1 Cell lines, plasmids, Abs, and reagents

Mouse WR19L cells (TIB-52; American Type Culture Collection [ATCC]) were grown in RPMI 1640 supplemented with 10% FCS. Human THP-1 cells (TIB-202; ATCC) were cultured in RPMI 1640 supplemented with 10% FCS and 55 µM 2-ME. HEK293T cells (CRL-1573; ATCC) were grown in DMEM containing 10% FCS.

The pNEF-BOS vector was derived from pEF-BOS (69), into which an SV40 early promotor-driven neomycin-resistance gene was introduced from pSV2-neo (70). The lentiCas9-Blast vector (71), mouse CRISPR Knockout Pooled Library (genome-scale CRISPR/Cas9 knockout [GeCKO] v2) (71), and pX330 and pX459v2 plasmids (72) were from Addgene. pCMV-vesicular stomatitis virus (VSV)-G-Rous sarcoma virus (RSV)-rev and pCMV-VSV-G (73) were provided by H. Miyoshi (RIKEN BioResource Center). The pMXs-puro retroviral vector (74) and the pGag-pol-IRES-bsr packaging plasmid (75) were from T. Kitamura (Institute of Medical Science, University of Tokyo). The pAdVAntage and pLVSIN-EF-1α lentiviral vectors were purchased from Thermo Fisher Scientific and Takara Bio, respectively.

The Alexa 488-conjugated rat anti-mouse P2X7 mAb (clone Hano43) was from Bio-Rad Laboratories. The HRP mouse anti-FLAG M2 mAb, anti-FLAG M2-conjugated magnetic beads, and $3\times$FLAG peptide were from Merck. The HRP rabbit anti-GFP Ab was from Medical & Biological Laboratories. The rabbit anti-rat P2X7 Ab was from Alomone Labs. The rabbit anti-human Eros Ab was from Atlas Antibodies. The mouse anti-Na$^+$/K$^+$-ATPase mAb (clone 464.6) was from Abcam. The HRP-goat anti-rabbit Igs Ab and the HRP-goat anti-mouse Igs Ab were from Agilent Technologies. The BzATP and ATP were purchased from Wako Pure Chemical and Nacalai Tesque, respectively. The BAPTA-AM and 1-[2-amino-5-(2,7-difluoro-6-acetoxymethoxy-3-oxo-9-xanthenyl)phenoxy]-2-(2-amino-5-methylphenoxy)ethane-N,N,N9,N9-tetraacetic acid, tetra(acetoxymethyl) ester (Fluo-4 AM) were from Dojindo Molecular Technologies. Cy5-labeled annexin V was from BioVision. Ionomycin and propidium iodide (PI) were from Merck. SYTOX Blue, YO-PRO-1, ER-Tracker Red and Hoechst 33342 were from Thermo Fisher Scientific. The 1-oleoyl-2-{6-[(7-nitro-2-1,3-benzoxadiazol-4-yl)amino]hexanoyl}-sn-glycero-3-phosphocholine (NBD-PC) was from Avanti Polar Lipids.

2.2 Gene editing and transformation of cell lines

The TMEM16F, P2X7, and Eros genes were knocked out using the CRISPR/Cas9 system and the pX330 or pX459v2 plasmid, as described previously (4, 72). Complementary oligonucleotides carrying the sgRNA target sequence were the following: mTMEM16F, 5'-GGATGAAGTCGATTCGCCTC-3'; mP2X7, 5'-TGAGCGATAAGCTGTACCAG-3'; mEros,

5'-ATTTGTGGCTGTACAGAACT-3'; hP2X7, 5'-TGATGACAGGCTCTTTCCGC-3'; and hEros, 5'-TGGAAGCTCTTCTACGTCAC-3'. The oligonucleotides were ligated into pX330 or pX459v2, and the resultant plasmid DNA was introduced into WR19L or THP-1 cells by electroporation using an NEPA21 Super Electroporator (Nepa Gene). In some cases, the transfection was carried out twice with a 3-d interval. At 20-30 h after transfection with the pX459v2 vector, the cells were treated with 1 μg/ml puromycin for 30 h. Single clones were isolated by limiting dilution and were genotyped by sequencing the sgRNA target region of the corresponding chromosomal gene.

To express P2X7 and Eros, the coding sequences for mP2X7k (FJ436444), mEros (NM_144832), hP2X7a (NM_002562), and hEros (NM_001100407) were prepared by RT-PCR using RNA from WR19L (mP2X7k andmEros), or THP-1 (hP2X7a and hEros) cells. These cDNAs were tagged with FLAG, hemagglutinin (HA), enhanced GFP (EGFP), or mCherry at the C terminus and inserted into pNEF-BOS (mP2X7k), pMXs-puro (mP2X7k and mEros), or pLVSIN-EF-1α (hP2X7a and hEros). The authenticity of the expression plasmids was confirmed by DNA sequencing. The expression plasmids constructed with the pNEF-BOS vector were digested singly with a restriction enzyme and introduced into WR19L cells by electroporation. Stable transformants were selected by culturing in the presence of 2 mg/ml G418. For viral transformation, pMXs-puro-based vectors were introduced into HEK293T cells together with pGag-pol-IRES-bsr, pCMV-VSV-G, and pAdVAntage, whereas pLVSIN-EF-1α-based vectors were introduced with pCAG-HIVgp and pCMV-VSV-G-RSV-rev. Retroviruses and lentiviruses in the culture supernatant were concentrated at 4°C by centrifugation at $6000 \times g$ for 16 h and used to infect WR19L and THP-1 cells, respectively. Transformants were selected in the presence of 1 μg/ml puromycin. If necessary, mP2X7-, EGFP-, or mCherry-positive cells were sorted using a FACSAria II (BD Biosciences).

2.3 Mice

The $Eros^{-/-}$ mice ($Cybc1^{tm1a(KOMP)/Mmucd}$) were obtained from the Mutant Mouse Resource and Research Centers and maintained on a C57BL/6N genetic background. All mice were housed in a specific pathogen-free facility at Research Institute for Microbial Diseases, Osaka University, and all mouse studies were approved by the Ethics Review Committee for Animal Experimentation of Research Institute for Microbial Diseases, Osaka University.

2.4 Flow cytometry for mP2X7, PtdSer exposure, NBD-PC, YO-PRO-1, and intracellular Ca^{2+}

To detect mP2X7 on WR19L cell transformants, 5×10^5 cells were washed with PBS containing 2% FCS (PBS/FCS), and incubated on ice for 30 min in 100 ml of PBS/FCS containing 40-fold-diluted Alexa 488-anti-mP2X7 mAb. The cells were then washed with PBS/FCS, suspended in 250 ml of PBS/FCS containing 250 nM SYTOX Blue, and analyzed by flow cytometry with a FACSCanto II (BD Biosciences). The data were analyzed by FlowJo software (BD Biosciences).

The P2X7-mediated PtdSer exposure was analyzed by annexin V binding, followed by flow cytometry, as described previously with slight modifications (9). In brief, cells were washed with PBS, resuspended in annexin buffer (10 mM HEPES-NaOH [pH 7.5], 140 mM NaCl, and 2.5 mM $CaCl_2$) containing 1000-fold-diluted, Cy5-labeled annexin V and 2.5 µg/ml PI, and preincubated at 20°C for 5 min or at 4°C for 10 min. The cells were then stimulated at 20°C or 4°C with ionomycin, BzATP, or ATP and analyzed by flow cytometry using a FACSCanto II. The P2X7-dependent internalization of PtdCho was assayed by the internalization of NBD-PC as described previously (9). In brief, 1.8×10^6 cells were suspended in 300 ml of annexin buffer and preincubated at 4°C for 10 min. Aliquots of 250 ml of the cell suspension were mixed with an equal volume of annexin buffer containing 500 nM NBD-PC and 1 mM ATP and incubated at 4°C. A 90-ml aliquot of this mixture was then mixed with 150 ml of annexin buffer containing 5 mg/ml fatty acid-free BSA, incubated on ice for 1 min, and analyzed with a FACSCanto II. The incorporation of YO-PRO-1 was similarly assayed by flow cytometry (76). In brief, 1.3×10^6 cells were preincubated at 4°C for 10 min in 650 ml of annexin buffer, mixed with 650 ml of annexin buffer containing 4 µM YO-PRO-1, 500 nM SYTOX Blue, and 1 mM ATP, incubated at 4°C, and analyzed with a FACSCanto II.

To monitor intracellular Ca^{2+}, 7×10^5 cells were incubated with 1.4 ml of 4 µM Fluo-4 AM in HEPES/NaCl buffer (10 mM HEPES-NaOH [pH 7.5] and 140 mM NaCl) at 25°C for 15 min, washed, incubated at 25°C for 15 min in 350 ml of HEPES/NaCl buffer, and chilled at 4°C for 10 min. A 150-ml aliquot of the cell suspension was then mixed with an equal volume of HEPES/NaCl buffer containing 5 mM $CaCl_2$, 500 nM SYTOX Blue, and 1 mM ATP, incubated at 4°C for 5 min, and analyzed by flow cytometry with a FACSCanto II.

2.5 Confocal microscopy

Cells stably expressing mP2X7k-EGFP, mEros-EGFP, and mEros-mCherry were washed with HBSS supplemented with 2% FCS (HBSS/FCS). The cells were suspended in HBSS/FCS containing 5 µg/ml Hoechst 33342, seeded into a glass-bottom dish (Matsunami), and observed by an FV1000-D confocal fluorescence microscope (Olympus). In some cases, cells were stained at 37°C for 15 min with 1 µM ER-Tracker Red before observing by microscope.

2.6 RT-PCR for mouse P2X7a and P2X7k

Several mouse tissues express two splice variants of P2X7, P2X7a, and P2X7k, which use a different exon 1 (77). To determine which variant is expressed in WR19L cells, the total RNA was prepared from the WR19L cells and the resident peritoneal macrophages of C57BL/6J mice using an RNeasy Mini Kit (QIAGEN), and reverse transcribed using SuperScript III Reverse Transcriptase (Thermo Fisher Scientific) or a High-Capacity RNA-to-cDNA Kit (Thermo Fisher Scientific). cDNA was subjected to PCR with PrimeSTAR GXL DNA Polymerase (Takara Bio) and the following primers:

specific forward primers, 5'-TTTTTAATTAAGCCACCATGCCGGCTTGCTGCAGCTG-3' on exon 1 for mP2X7a and 5'-TTTTTAATTAAGCCACCATGCTGCCCGTGAGCCAC-3' on exon 1' for mP2X7k, and a common reverse primer, 5'-AAAGAATTCGTAGGGATACTTGAAGCCAC-3' on exon 13.

2.7 Genome-wide CRISPR screening

Genome-wide CRISPR screening was carried out essentially as described previously (78, 79). In brief, *TMEM16F$^{-/-}$P2X7$^{-/-}$(DKO)* WR19L cells established by the CRISPR/Cas9 system were stably transformed with pNEF-BOS-mP2X7k to generate *DKO*-WR19L-mP2X7k cells. A lentivirus-carrying Cas9-FLAG was produced by transfecting HEK293T cells with lentiCas9-Blast, pCAG-HIVgp, and pCMV-VSV-G-RSV-rev, and was used to infect *DKO*-WR19L-mP2X7k cells. Transformants were selected in the presence of 10 µg/ml blasticidin S, and the clone expressing Cas9-FLAG was identified by Western blotting with anti-FLAG. The lentivirus for the sgRNA library was produced by transfecting HEK293T cells (1×10^7) with 17 µg of GeCKO v2 library (A and B) DNA, 8 µg pCAG-HIVgp, and 5 µg pCMV-VSV-G-RSV-rev and concentrated at 4°C by centrifugation at $6000 \times g$ for 16 h. This virus was used to infect *DKO*-WR19L-mP2X7k/Cas9 cells at a multiplicity of infection of 0.3. In brief, 2×10^7 cells in 48-well plates at 4×10^5 cells per well were spin infected at $700 \times g$ for 1 h at 30°C in the presence of 10 µg/ml polybrene. The cells were then cultured for 4 d in medium containing 1 µg/ml puromycin and 800 µg/ml G418, with one passage with a 3-fold dilution. The cells were then cultured without the antibiotics for 2 d, during which they were passaged once with a 4-fold dilution.

The resulting *DKO*-WR19L-mP2X7k/Cas9/GeCKO cells (3×10^7) were washed with PBS, resuspended in 2 ml of annexin buffer, and chilled at 4°C for 10 min. One milliliter of chilled annexin buffer containing 180 µM BzATP was then added to the cells, and the mixture was incubated at 4°C for 5 min. After a 15-fold dilution with chilled annexin buffer, the cells were collected by centrifugation at 4°C at $300 \times g$ for 3 min, suspended in 3 ml of annexin buffer containing 1000-fold-diluted, Cy5-labeled annexin V and 2.5 µg/ml PI, and subjected to cell sorting with a FACSAria II. The cell population with the lowest annexin V signal (~0.8%) was collected and cultured for 3 d in the presence of 800 µg/ml G418 and for 2 d in the absence of G418. This procedure (stimulation with BzATP, sorting of the cells expressing low levels of PtdSer, and expansion) was performed three times.

Genomic DNA was prepared from the third-sorted cells using the QIAamp DNA Mini Kit (QIAGEN), and a portion of the integrated lentiviral DNA carrying the sgRNA sequence was amplified by PCR using PrimeSTAR GXL DNA Polymerase and primers (5'-AATGGACTATCATATGCTTACCGTAACTTGAAAGTATTTCG-3' and 5'-CTTTAGTTTGTATGTCTGTTGCTATTATGTCTACTATTCTTTCC-3'). The PCR product was

then subjected to PCR using PrimeSTAR HS DNA polymerase (Takara Bio) to attach adaptor sequences for next-generation sequencing (NGS) with a mixture of forward primers (NGS-Lib-Fwd-1-10) (79) and a common reverse primer (5'-CAAGCAGAAGACGGCATACGAGATGTGACTGGAGTTCAGACGTGTGCTCTTCCGATC TTCTACTATTCTTTCCCCTGCACTGT-3'). The resultant PCR product was purified using spin columns (Promega), quantified with a Quant-iT PicoGreen dsDNA Assay Kit (Thermo Fisher Scientific), and analyzed by NGS with MiSeq (Illumina) using the MiSeq Reagent Kit v3 (Illumina). The obtained reads were linked to the corresponding sgRNA sequence, and the abundance of each unique sgRNA was calculated using software that was custom prepared at Amelieff.

2.8 Preparation of whole-cell lysates and membrane fractions

Whole-cell lysates were prepared by rotating cells at 4°C for 1 h in 50 mM Tris-HCl buffer (pH 7.5) containing 1% NP-40, 150 mM NaCl, and a protease inhibitor mixture (cOmplete, EDTA-free; Roche). The insoluble materials were removed by centrifugation at 4°C, $20,000 \times g$, for 20 min.

To prepare the membrane fractions from WR19L cells, 2.5×10^7 cells were washed with PBS and then homogenized on ice in 2.7 ml of solution A [10 mM Tris-HCl (pH 7.5) and 1 mM (p-amidinophenyl)methanesulfonyl fluoride hydrochloride (p-APMSF)] using a Dounce homogenizer. After adding 2.7 ml of solution B (10 mMTris-HCl [pH 7.5], 500 mM sucrose, 100 mM KCl, 10 mM $MgCl_2$, and 1 mM p-APMSF) to the homogenate, the nuclei and mitochondria were removed at 4°C by sequential centrifugations at $800 \times g$ for 10 min and at $8000 \times g$ for 10 min. The membrane fractions were then precipitated by centrifugation at $100,000 \times g$ for 60 min and suspended in 600 µl of 20 mM Tris-HCl buffer (pH 7.5) containing 1% n-dodecyl-β-D -maltopyranoside (DDM), 50 mM KCl, 1 mM $MgCl_2$, 10% glycerol, 1 mM p-APMSF, and a protease inhibitor mixture (cOmplete, EDTA-free). The suspensions were homogenized by passing them through a 29G needle and solubilized by rotation at 4°C for 2 h. The insoluble materials were removed by centrifugation at $20,000 \times g$ for 20 min, and the supernatant was used as the crude membrane fraction.

To prepare the membrane fraction from THP-1 cells, 1.3×10^7 cells were treated with 120 ng/ml PMA for 3 d, and cultured for another 3 d without PMA. After washing with PBS, the cells were collected with a cell scraper and suspended in 2.5 ml of solution A. The cells were lysed with an ultrasonic liquid processor (Q55; Qsonica). After adding 2.5 ml of solution B, the membrane fraction was prepared as described above, and solubilized in 200 ml of 50 mM Tris-HCl buffer (pH 7.5) containing 1% NP-40, 150 mM NaCl, and a protease inhibitor mixture (cOmplete, EDTA-free).

2.9 Immunoprecipitation, SDS-PAGE, Blue native PAGE, and Western blotting

To immunoprecipitate the mP2X7-mEros complex, 500 µl of crude membrane lysate (60 µg protein)

from WR19L cell transformants expressing mP2X7-FLAG and mEros-EGFP was incubated at 4°C overnight with 10 μl (bed volume) of anti-FLAG M2 magnetic beads. After washing three times with 1 ml of 20 mM Tris-HCl buffer (pH 7.5) containing 0.05% DDM, 50 mM KCl, 1 mM MgCl$_2$, and 10% glycerol, proteins bound to the beads were eluted with 150 μg/ml 3$\times$FLAG peptide in 100 ml of 20 mM Tris-HCl buffer (pH 7.5) containing 1% DDM, 50 mM KCl, 1 mM MgCl$_2$, and 10% glycerol.

For SDS-PAGE, whole-cell lysates or crude membrane lysates were incubated for 1 h at room temperature in SDS sample buffer (62.5 mM Tris-HCl [pH 6.8], 2% SDS, 10% glycerol, 2.5% 2-ME, and 0.005% bromophenol blue) and separated by electrophoresis on a 7.5% or 15% polyacrylamide gel (Nacalai Tesque). Precision Plus Protein Dual Color Standards (Bio-Rad Laboratories) were used as m.w. markers. For Blue native PAGE (BN-PAGE), samples were mixed with NativePAGE Sample Buffer (4$\times$) and NativePAGE 5% G-250 Sample Additive (20$\times$) and loaded onto a NativePAGE Novex 4-16% BisTris gel (Thermo Fisher Scientific). After electrophoresis at 150 V for 35 min at 4°C, the concentration of Coomassie Brilliant Blue (CBB) G-250 in the running buffer was changed from 0.02 to 0.002%, and the samples were subjected to further electrophoresis successively at 150 V for 25 min, 250 V for 30 min, and 350 V for 20 min. The NativeMark Unstained Protein Standard (Thermo Fisher Scientific) was used as m.w. markers.

For Western blotting, separated proteins in a gel were transferred to a polyvinylidene difluoride membrane (MilliporeSigma) immediately after SDS-PAGE or after incubating a BN-PAGE gel in SDS-PAGE running buffer (25 mM Tris-HCl [pH 8.3], 192 mM glycine, and 0.1% SDS) for 15 min at room temperature. The membranes were blocked with 5% skim milk and probed with HRP-labeled Abs, followed by detection with the Immobilon Western Chemiluminescent HRP substrate (Merck). Proteins on the polyvinylidene difluoride membrane were stained with CBB R-250 as a loading control.

2.10 IL-1β ELISA

THP-1 cells were treated with PMA to promote their differentiation to macrophages, and ATP-induced IL-1β secretion was performed as described previously (59, 80) with slight modification. In brief, THP-1 cells at a density of 2.5×10^5 cells per well in 24-well plates were cultured in RPMI 1640 containing 10% FCS and 120 ng/ml PMA for 3 d. The PMA was removed, and the cells were further cultured successively for 2 d in RPMI 1640-10% FCS, and overnight in the same medium containing 100 ng/ml LPS. The cells were then stimulated for 5 h with 1-3 mM ATP in RPMI 1640-10% FCS. The culture medium was centrifuged at 4°C, 20,000$\times$g for 15 min, and IL-1β in the supernatant was quantified using an ELISA kit (Quantikine ELISA Human IL-1β/IL-1F2; R&D Systems).

For bone marrow-derived macrophages (BMDMs), bone marrow was prepared from the femurs

of 3-wk-old, wild-type $Eros^{+/+}$ and $Eros^{-/-}$ littermate mice and treated with RBC Lysis Buffer (Buffer EL; QIAGEN). The cells were cultured for 4 d in RPMI 1640 supplemented with 10% FCS, 55 μM 2-ME, and 10% of medium conditioned with CMG14-12 (81) (Medium M) by changing the medium every other day. The macrophages were suspended in PBS containing 1 mM EDTA using cell scrapers and collected by centrifugation at $300 \times g$ for 3 min. The cells were suspended in Medium M, and 7.5×10^4 cells per well were cultured in 48-well plates. One day later, the cells were primed with 100 ng/ml LPS for 3 h and stimulated for 6 h with ATP. The culture medium was centrifuged at $20,000 \times g$ for 15 min at 4°C, and IL-1β in the supernatant was quantified using an ELISA kit (Quantikine ELISA Mouse IL-1β/IL-1F2; R&D Systems).

3. Result

3.1 P2X7-dependent, but TMEM16F-independent, PtdSer exposure

Ousingsawat et al. (68) reported that P2X7-induced PtdSer exposure is mediated by a Ca^{2+}-dependent scramblase, TMEM16F. I examined this possibility using a mouse cell line derived from WR19L T cell lymphoma. WR19L cells that were stimulated at 20°C with 3 μM ionomycin exposed PtdSer within 5 min (Fig. 1A, 1B). As Suzuki et al. previously reported (11), this PtdSer exposure was completely inhibited by chelating the intracellular Ca^{2+} with 25 μM BAPTA-AM (Fig. 1A), and it was not observed in $TMEM16F^{-/-}$ ($16F^{-/-}$) WR19L cells (Fig. 1B) prepared by the CRISPR/Cas9 system (Supplemental Fig. 1A). Treating WR19L cells at 20°C for 5 min with 300 μM BzATP, an agonist for P2X7 (82), strongly increased the PtdSer exposure (Fig. 1A). As expected, BzATP did not induce the PtdSer exposure in $P2X7^{-/-}$ WR19L cells (Fig. 1B, Supplemental Fig. 1B). However, in contrast to the proposal by Ousingsawat et al. (68), the null mutation of TMEM16F had little effect on the BzATP-induced PtdSer exposure (Fig. 1B). Furthermore, preincubating WR19L cells with BAPTA-AM had no effect on the BzATP-induced PtdSer exposure (Fig. 1A), indicating that other TMEM16 family members with Ca^{2+}-dependent scrambling activity (11) were probably not involved in this process. From these results, I concluded that the P2X7-induced PtdSer exposure in WR19L cells proceeds independently from the TMEM16F-mediated phospholipid scrambling.

3.2 Screen for molecules that support P2X7-mediated PtdSer exposure

There are several alternatively spliced forms of mP2X7 mRNA (83), two of which (P2X7a and P2X7k) are found in the thymus and spleen (77, 84). To examine which splice variants were expressed in WR19L cells, their RNA was subjected to RT-PCR for the P2X7a and P2X7k isoforms. As reported previously (84), the mouse macrophages exclusively expressed P2X7a mRNA, whereas WR19L cells predominantly expressed the P2X7k isoform (Fig. 2A). To confirm the contribution of

10

mP2X7k to the BzATP-induced PtdSer exposure, *TMEM16F$^{-/-}$P2X7$^{-/-}$* (*DKO*)-WR19L cells were established using the CRISPR/Cas9 system (Supplemental Fig. 1B). As expected, the *DKO*-WR19L cells did not respond to ionomycin or BzATP (Fig. 1B). Transforming the *DKO*-WR19L cells with mP2X7k (*DKO*-mP2X7k) resulted in a high expression of mP2X7k on their cell surface (Fig. 2B) and strongly sensitized the cells to the BzATP-induced PtdSer exposure. That is, three times less concentration of BzATP than that for the wild-type cells was sufficient to activate the mP2X7k-transformed cells to expose PtdSer at 20°C for 5 min in the absence of TMEM16F, confirming that TMEM16F was not required for the P2X7-mediated PtdSer exposure.

To identify molecules that were required for the P2X7-mediated PtdSer exposure, *DKO*-mP2X7k cells were subjected to a CRISPR screen (78) (Fig. 2C). In this screen, a clone of the mP2X7k transformants that strongly and universally exposed PtdSer in response to 60 μM BzATP at 4°C for 5 min was identified by limiting dilution and cell sorting. The cloned cells were transformed with Cas9, and were infected with a lentivirus carrying a GeCKO library (71) at a multiplicity of infection of 0.3 to achieve <1 sgRNA-carrying lentivirus per host cell. The cells were then stimulated with 60 μM BzATP at 4°C for 5 min, and a 0.8% population that severely lost the ability to expose PtdSer was isolated by cell sorting (Fig. 2C). This sorting of cells that lost the ability to expose PtdSer in response to BzATP was repeated two more times. Flow cytometry analysis indicated that after the third sorting, some cell population almost fully lost the ability to expose PtdSer in response to BzATP (Fig. 2C). A deep sequencing analysis of the chromosomal DNA of the sorted cell population indicated that the sgRNAs for Eros (CYBC1) were the most enriched, suggesting that Eros was required for the P2X7-mediated PtdSer exposure.

3.3 Requirement of Eros for P2X7-mediated processes

To confirm that Eros was involved in the P2X7-mediated PtdSer exposure, the Eros in *DKO*-mP2X7k was knocked out by the CRISPR/Cas9 system (Supplemental Fig. 1C). The ability of the resultant cell line (*TKO*-mP2X7k) to expose PtdSer in response to BzATP or ATP was severely impaired, and this impairment was fully rescued by transforming the cells with mEros (*TKO*-mP2X7k/mEros) (Fig. 3A). P2X7 mediates not only PtdSer exposure, but also ATP-induced phospholipid scrambling (85), dye uptake (86), Ca^{2+} influx (50, 87), and IL-1β production (88). Accordingly, stimulating *DKO*-mP2X7k, but not *DKO*, cells with ATP promoted phospholipid scrambling, assayed by the incorporation of NBD-PC (Fig. 3B). This activity was not observed in *TKO*-mP2X7k cells and was rescued by transforming these cells with Eros. Similarly, ATP promoted the incorporation of YO-PRO-1 in *DKO*-mP2X7k cells. This effect was decreased in *TKO*-mP2X7k, and transforming *TKO* cells with mEros together with mP2X7 strongly increased the incorporation of YO-PRO-1. Furthermore, *DKO* cells did not respond to ATP for Ca^{2+} internalization, but *DKO*-mP2X7k cells responded well to ATP, and the intracellular Ca^{2+}, detected by the Fluo-4 Ca^{2+}

sensor, increased within 5 min after the ATP treatment (Fig. 3D). This response was not observed in *TKO*-mP2X7k cells, but was rescued by expressing mEros in *TKO*-mP2X7k/mEros cells.

hP2X7 has 81.3% aa sequence identity with mP2X7. As previously reported (59), human THP-1-derived macrophages primed with LPS dose dependently responded to ATP to produce IL-1β (Fig. 3E). To examine the contribution of Eros in this process, the Eros and P2X7 genes in THP-1 cells were individually knocked out by the CRISPR/Cas9 system (Supplemental Fig. 2). As shown in Fig. 3E, not only the P2X7-null mutation, but also the Eros-null mutation completely blocked the IL-1β production, and this defect was rescued by expressing hP2X7 or hEros, respectively.

I then prepared BMDMs from wild-type and *Eros*^{-/-} mice. Consistent with previous reports (55, 63), the LPS-primed, wild-type BMDMs produced IL-1β in response to ATP (Fig. 3F). In contrast, *Eros*^{-/-} BMDMs almost completely lost the ability to produce IL-1β in response to ATP (Fig. 3F). From these results, I concluded that various P2X7-mediated biological processes in mouse and human cells require Eros.

3.4 Chaperone-like activity of Eros for P2X7 expression

Eros was recently shown to be required for the stable expression of the NADPH oxidase subunits gp91[phox] and p22[phox] by acting as a chaperone (89). To examine whether Eros acts as a chaperone for P2X7, FLAG-tagged mP2X7k was introduced into *DKO*, *TKO*, and *TKO*-mEros cells, and the mP2X7k expression was evaluated by Western blotting with anti-P2X7 Ab. As shown in Fig. 4A, mP2X7k was stably expressed in *DKO* cells. However, its expression was severely reduced in *TKO* cells, and this decrease was rescued by transforming the cells with mEros. Similar results were obtained for endogenous hP2X7 in THP-1 cells. Western blotting with anti-P2X7 Ab detected bands of 75 and 200 kDa in the membrane fraction from the wild-type, but not *P2X7*^{-/-}THP-1, cells. The intensity of these bands increased by transforming the cells with hP2X7-FLAG (Fig. 4B), indicating that these bands corresponded to the monomer and trimer forms of hP2X7. The expression of hP2X7 was severely decreased by the null mutation of Eros, and this reduction was fully rescued by expressing hEros. Similarly, the wild-type (*Eros*^{+/+}) BMDMs expressed a high level of P2X7 (Fig. 4C). This expression was not reduced by the heterozygous null mutation of Eros (*Eros*^{+/-}) but severely reduced by the homozygous null mutation (*Eros*^{-/-}).

The requirement of Eros for the cell-surface expression of P2X7 was then examined with WR19L cells. Flow cytometry analysis with anti-mP2X7 Ab showed that mP2X7 was highly expressed in the *DKO*-mP2X7k cells. In contrast, mP2X7 on the surface of *TKO*-mP2X7k cells was severely decreased, but it was fully rescued in *TKO*-mP2X7k/mEros cells (Fig. 4D). To examine the localization of mP2X7 and mEros, mP2X7k and mEros were fused with EGFP, and expressed in *TKO* cells together with mEros-HA or mP2X7-FLAG, respectively. Observation by confocal microscopy indicated that a substantial portion of the mP2X7k was localized to the plasma

membrane (Fig. 4E). In contrast, in agreement with a previous report (89), the mEros-EGFP in *TKO*-mP2X7k cells was exclusively observed intracellularly, and merged well with the ER-Tracker, indicating that mEros is localized at endoplasmic reticulum. When *TKO* cells were transformed to coexpress mP2X7k-EGFP and mEros-mCherry, the intracellular EGFP signal was colocalized with mCherry signals (Fig. 4F), suggesting that mEros assisted the folding or maturation of mP2X7 at the endoplasmic reticulum and that the mature mP2X7 moved to the plasma membrane. To test this possibility, *DKO*, *TKO*, and *TKO*-mEros-EGFP cells were transformed with FLAG-tagged mP2X7k, and their membrane fractions were analyzed by BN-PAGE. As shown in Fig. 4G, Western blotting with anti-FLAG Ab showed two bands at around 800 and 550 kDa in the *DKO* and *TKO*-mEros, but not in the *TKO* cells. The lower band at 550 kDa appeared to correspond to a trimeric form of mP2X7k, as reported previously (77). The anti-GFP Ab for mEros-EGFP detected two bands, of which the upper one was similar to the upper band observed with the anti-FLAG Ab for mP2X7k. The membrane fraction was then subjected to immunoprecipitation with anti-FLAG beads for the mP2X7k-FLAG. As shown in Fig. 4H, the precipitates carried the upper large complex, which could be recognized not only with the anti-FLAG for mP2X7k, but also with the anti-GFP for mEros. These results indicated that the large band of 800 kDa was a complex between mP2X7k and mEros in the endoplasmic reticulum. Mature mP2X7k with an apparent Mr of 550 kDa was present on the plasma membrane, whereas mEros, free or complexed with other proteins, was present in the endoplasmic reticulum. I concluded that mEros transiently interacts with mP2X7 at the endoplasmic reticulum and assists its folding. mP2X7 then moves to the plasma membrane, where it is present as a homotrimeric complex.
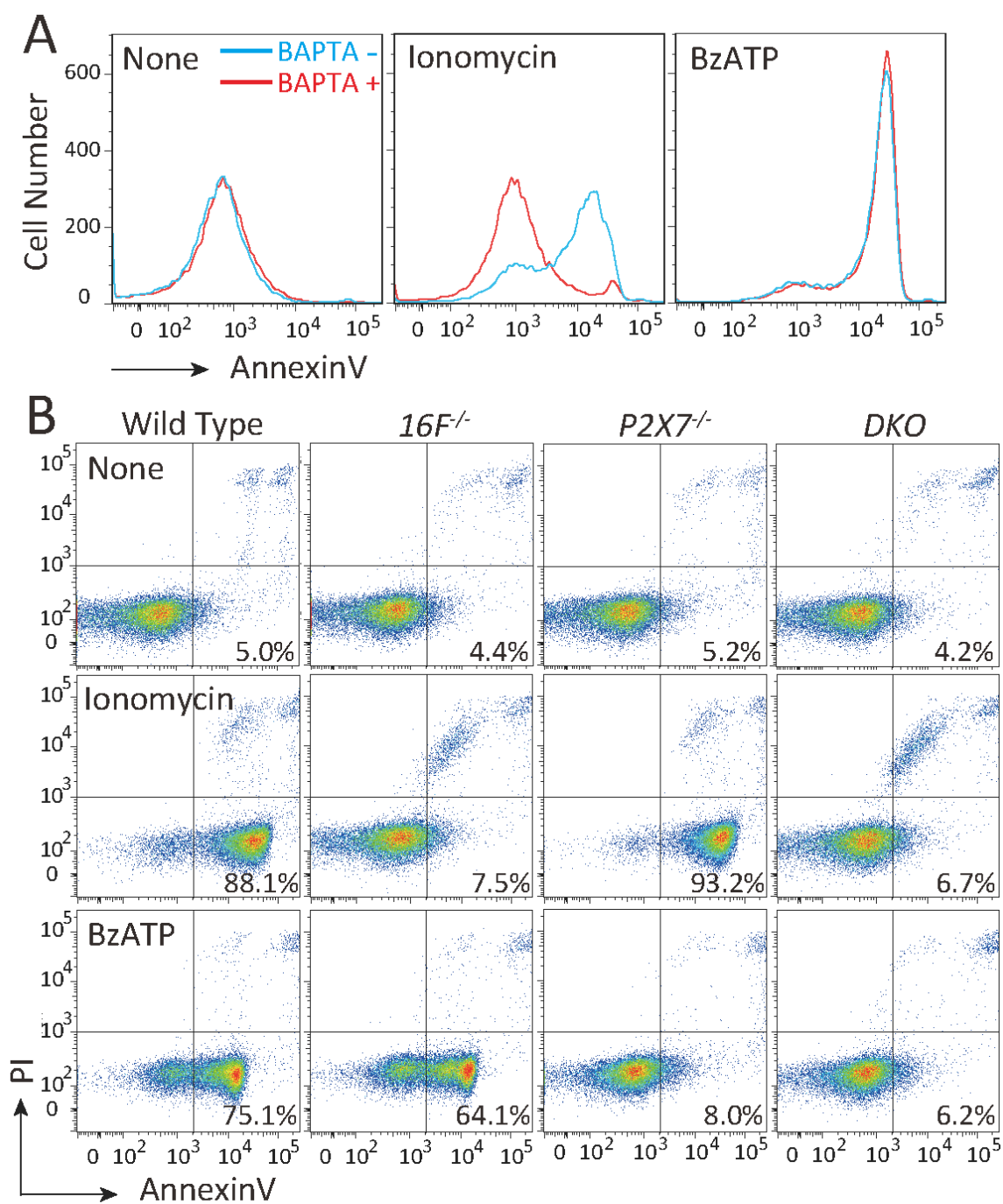
4. Figures

Figure 1. P2X7-mediated, TMEM16F-independent PtdSer exposure in WR19L cells.

(A) Ca^{2+} is not required for BzATP-induced PtdSer exposure in WR19L cells. After preincubation at 25°C for 15 min with or without 25 μM BAPTA-AM, the WR19L cells were left untreated or stimulated at 20°C for 5 min with 3 μM ionomycin or 300 μM BzATP. The cells were then stained with Cy5-labeled annexin V in the presence of 2.5 μg/ml PI and analyzed by flow cytometry. Annexin V staining in the PI-negative population is shown. (B) TMEM16F-dependent or P2X7-dependent PtdSer exposure in WR19L cells. The wild-type, $TMEM16F^{-/-}$ ($16F^{-/-}$), $P2X7^{-/-}$, and $16F^{-/-}P2X7^{-/-}$ (*DKO*) WR19L cells were stimulated with ionomycin or BzATP as described above, stained with annexin V and PI, and analyzed by flow cytometry.
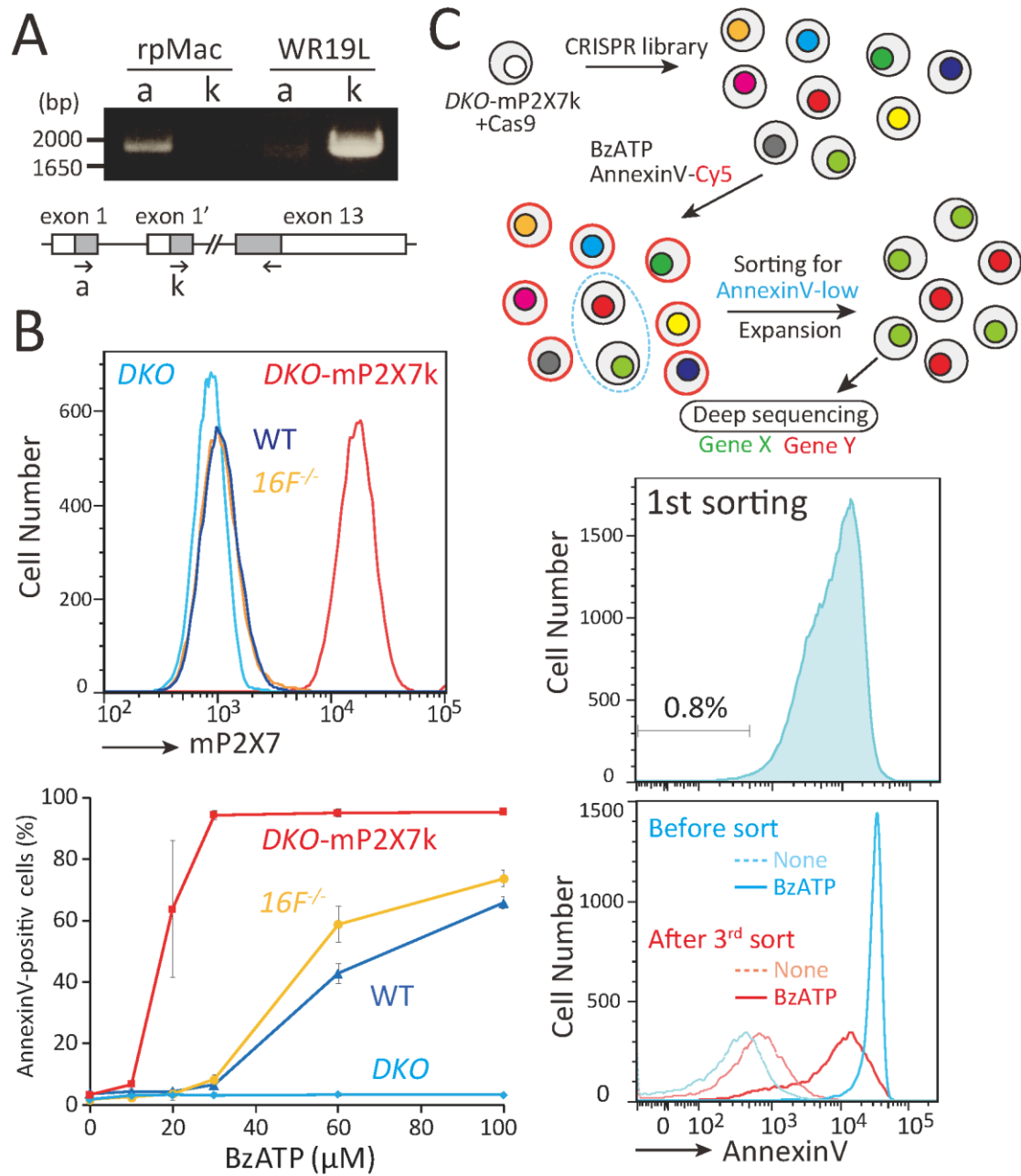
Figure 2. Genome-wide CRISPR screen for genes that support P2X7-mediated PtdSer exposure.

(A) Predominant expression of the P2X7k isoform in WR19L cells. The transcripts for the P2X7a and P2X7k isoforms were detected by RT-PCR in RNA from mouse resident peritoneal macrophages (rpMacs) and WR19L cells. In the lower panel, the structure of the mP2X7 gene is shown schematically with the positions of primers. The P2X7a and P2X7k isoforms were generated by alternative use of the first exon (exon 1 and exon 19). Forward primers on the first exon were specific for each isoform, whereas the reverse primer on exon 13 was common. (B) mP2X7k-mediated PtdSer exposure. In the upper panel, wild-type (WT), $16F^{-/-}$, DKO, and *DKO*-mP2X7k cells were stained with Alexa 488-anti-mP2X7 Ab and analyzed by flow cytometry. Staining profiles in the SYTOX Blue-negative population are shown. In the lower panel, WT, $16F^{-/-}$, *DKO*, and *DKO*-P2X7k cells were treated at 20°C for 5 min with the indicated concentration of BzATP, stained with Cy5-labeled annexin V, and analyzed by flow cytometry. The experiments were performed three times, and the average percentage of annexin V-positive cells in the PI-negative population was plotted with SD (bars). (C) Identification of a gene that supports mP2X7-mediated PtdSer exposure. The upper panel shows the CRISPR-screening procedure. In the first step, *DKO*-P2X7k cells were transformed with Cas9 and the CRISPR library, and a population of cells with a reduced activity for BzATP-induced PtdSer exposure was sorted three times. In the second step, DNA from these sorted cells was subjected to deep sequencing, and the read sequences were processed to determine the abundance of each sgRNA. The middle panel shows the FACS profile of the first sorting, in which the population sorted for the next step is indicated. In the lower panel, the original cells and cells after the third sorting were left unstimulated or stimulated with BzATP and analyzed by flow cytometry. The annexin V-staining profiles in the PI-negative population are shown.

A

DKO-mP2X7k   *TKO*-mP2X7k   *TKO*-mP2X7k/mEros

None
1.8%   1.0%   0.6%

BzATP
88.0%   24.3%   91.7%

ATP
89.7%   20.9%   90.9%

PI / AnnexinV

B

NBD-PC (×10³ MFI)

TKO-mP2X7k/mEros
DKO-mP2X7k
TKO-mP2X7k
DKO

Time (min)

C

YO-PRO-1 (RFI)

TKO-mP2X7k/mEros
DKO-mP2X7k
TKO-mP2X7k
DKO

Time (min)

D

DKO   *DKO*-mP2X7k   *TKO*-mP2X7k   *TKO*-mP2X7k/mEros

Cell Number
None
ATP

Fluo4

E

IL-1β (pg/mL)

| ATP (mM) | 0 1 2 3 | 0 1 2 3 | 0 1 2 3 | 0 1 2 3 | 0 1 2 3 | 0 1 2 3 | 0 1 2 3 | 0 1 2 3 | 0 1 2 3 | 0 1 2 3 |
| LPS | − | + | − | + | − | + | − | + | − | + |

Wild Type   *Eros⁻/⁻*   *Eros⁻/⁻*-hEros   *P2X7⁻/⁻*   *P2X7⁻/⁻*-hP2X7

F

IL-1β (pg/mL)

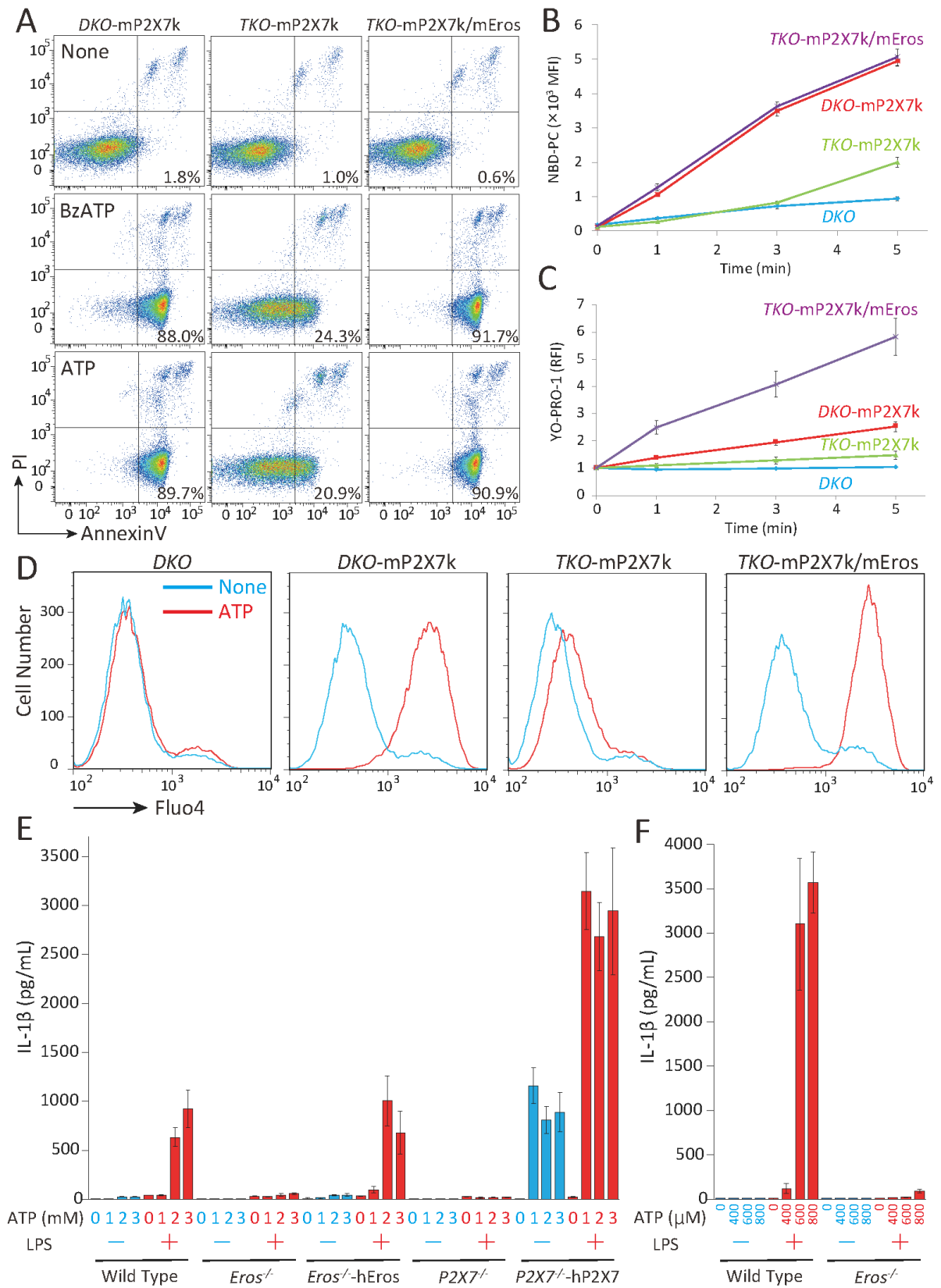| ATP (μM) | 0 400 600 800 | 0 400 600 800 | 0 400 600 800 | 0 400 600 800 |
| LPS | − | + | − | + |

Wild Type   *Eros⁻/⁻*

18

Figure 3. Essential role of Eros for P2X7-mediated signal transduction.

(A) Effect of mEros on mP2X7k-mediated PtdSer exposure. *DKO*-mP2X7k, *TKO*-mP2X7k, and *TKO*-mP2X7k/mEros cells were stimulated at 4°C for 5 min with 60 μM BzATP or 500 μM ATP, stained with annexin V, and analyzed by flow cytometry. (B and C) Effect of mEros on the mP2X7k-mediated internalization of PtdCho and YO-PRO-1. *DKO*, *DKO*-mP2X7k, *TKO*-mP2X7k, and *TKO*-mP2X7k/mEros cells were stimulated at 4°C with 500 μM ATP for the indicated time in the presence of 250 nM NBD-PC (B) or 2 μM YO-PRO-1 (C). The mean fluorescence intensity (MFI) of the BSA-nonextractable NBD-PC or the incorporated YO-PRO-1 in the SYTOX Blue-negative population was determined. These experiments were carried out three times, and the average MFI or its relative value (relative fluorescence intensity [RFI]) was plotted with SD (bars). (D) Effect of mEros on the mP2X7k-mediated Ca^{2+} influx. *DKO*, *DKO*-mP2X7k, *TKO*-mP2X7k, and *TKO*-mP2X7k/mEros cells were loaded with Fluo-4 AM and stimulated with 500 μM ATP at 4°C for 5 min. The Fluo-4 fluorescence profiles in the SYTOX Blue-negative population are shown. (E) Effect of hEros on ATP-induced IL-1β secretion in THP-1 cells. After being treated with PMA, wild-type THP-1, *Eros*^{-/-}, *Eros*^{-/-}-hEros, *P2X7*^{-/-}, and *P2X7*^{-/-}-hP2X7a cells were incubated at 37°C overnight with (+) or without (-) 100 ng/ml LPS and cultured for 5 h in the presence of the indicated concentrations of ATP. IL-1β in the culture medium was measured by ELISA. The experiments were carried out in triplicate, and the average values were shown with SD (bars). (F) Requirement of Eros in the ATP-triggered IL-1β secretion in mouse BMDMs. BMDMs from wild-type and *Eros*^{-/-} mice were incubated at 37°C for 3 h + or - 100 ng/ml LPS and cultured for 6 h in the presence of the indicated concentrations of ATP. IL-1β in the culture medium was measured by ELISA. The experiments were carried out in triplicate, and the average values were shown with SD (bars).
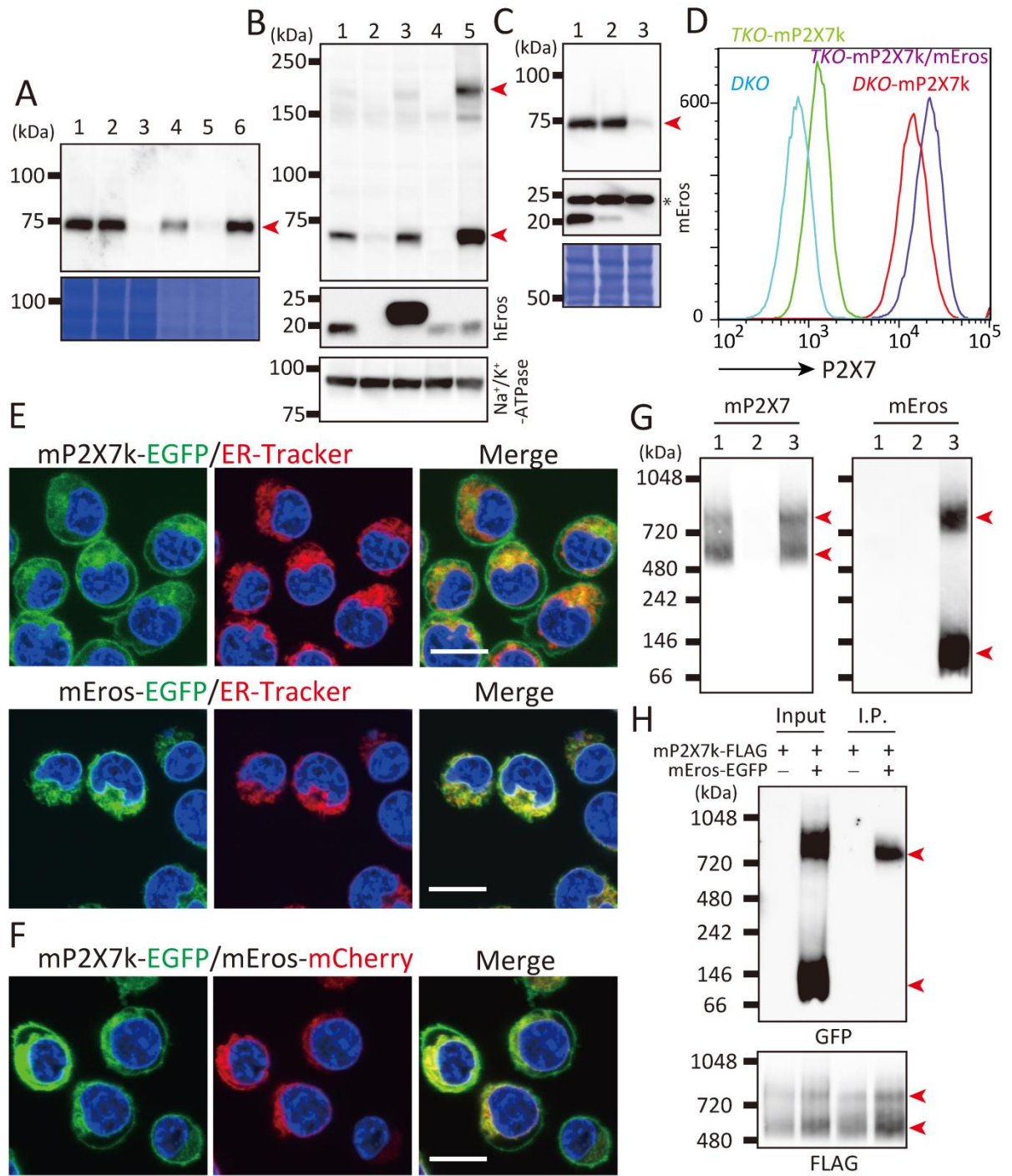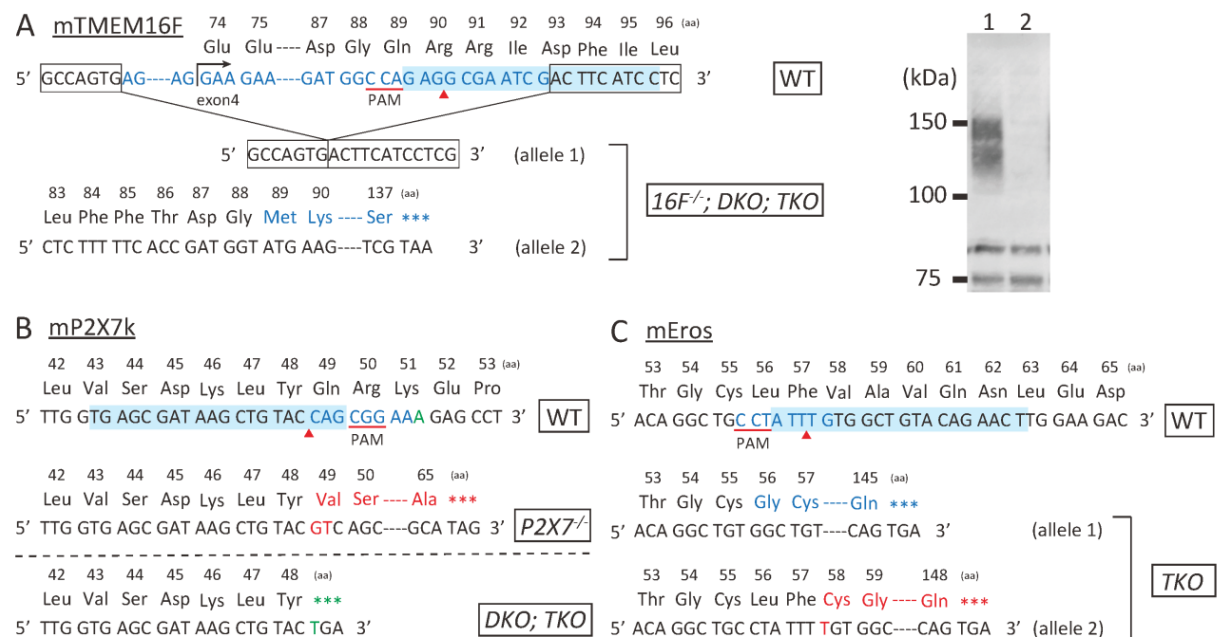
Figure 4. Requirement of Eros for the cell-surface expression of P2X7.

(A) Effect of mEros on the expression of exogenously introduced mP2X7k in WR19L cells. Cell lysates from wild-type (lane 1), $16F^{-/-}$ (lane 2), *DKO* (lane 3), *DKO*-mP2X7k-FLAG (lane 4), *TKO*-mP2X7k-FLAG (lane 5), and *TKO*-mP2X7k-FLAG/mEros cells (lane 6) were separated by SDS-PAGE (5 mg of protein for lane 1–3 and 0.5 mg of protein for lane 4–6) and analyzed by Western blotting with anti-P2X7 Ab. At the bottom, the membrane was stained with CBB R-250. Arrowhead indicates monomeric form of mP2X7. (B) Effect of hEros on the endogenous P2X7 expression in THP-1 cells. Wild-type (lane 1), $Eros^{-/-}$ (lane 2), $Eros^{-/-}$-hEros-HA (lane 3), $P2X7^{-/-}$ (lane 4), and $P2X7^{-/-}$-hP2X7a-FLAG cells (lane 5) were treated with PMA. Crude membranes (7.5 mg of protein) were solubilized with 1% NP-40, separated by SDS-PAGE, and analyzed by Western blotting with anti–P2X7 Ab. At the bottom, the membrane was probed with anti-Eros or anti–Na^+/K^+-ATPase Ab. Arrowheads indicate trimeric and monomeric forms of hP2X. (C) Effect of Eros on the endogenous P2X7 expression in mouse primary macrophages. Cell lysates of BMDMs from wild-type (lane 1), $Eros^{+/-}$ (lane 2), and $Eros^{-/-}$ (lane 3) mice were separated by SDS-PAGE (12.5 mg of protein) and analyzed by Western blotting with anti-P2X7 Ab. At the bottom, the membrane was probed with anti-Eros Ab or stained with CBB R-250. Arrowhead indicates monomeric form of mP2X7, and asterisk indicates nonspecific bands. (D) Effect of mEros on the cell-surface expression of mP2X7k in WR19L cells. *DKO*, *DKO*-mP2X7k, *TKO*-mP2X7k, and *TKO*-mP2X7k/mEros cells were stained with Alexa 488-anti-mP2X7 Ab. The Alexa 488-staining profiles in the SYTOX Blue–negative population are shown. (E and F) Subcellular distribution of mP2X7k and mEros. *TKO*-WR19L cells were transformed with mP2X7k-EGFP and mEros, or with mP2X7k and mEros-EGFP, and stained by ER-Tracker Red (E), or transformed with mP2X7k-EGFP and mEros-mCherry (F), and observed by confocal microscopy in the presence of 5 mg/ml Hoechst 33342. EGFP, ER-Tracker Red or mCherry, and Hoechst signals are shown in green, red, and blue, respectively. Scale bar, 10 μm (G) BN-PAGE analysis of mP2X7 and mEros. Crude membrane fractions (1.2 mg protein) from *DKO*-mP2X7k-FLAG (lane 1), *TKO*-mP2X7k–FLAG (lane 2), and *TKO*-mP2X7k-FLAG/mEros-EGFP cells (lane 3) were solubilized with 1% DDM, separated by BN-PAGE, and analyzed by Western blotting with anti-FLAG (left panel) or anti-GFP Ab (right panel). (H) Coimmunoprecipitation of mEros with mP2X7k. Crude membranes (60 mg protein) from *DKO*-mP2X7k-FLAG or *TKO*-mP2X7k-FLAG/mEros-EGFP cells were solubilized with 1% DDM. The FLAG-tagged protein was immunoprecipitated with anti-FLAG M2 magnetic beads and eluted with 3×FLAG peptide. The crude membrane lysates (1.5 mg protein) (Input) and 1/16 of the eluates (I.P.) were separated by BN-PAGE and analyzed by Western blotting with anti-GFP (top panel) or anti-FLAG Ab (bottom panel).

Supplemental Figure 1. Gene knock-out in WR19L cells by CRISPR-Cas9 system.
The wild-type and mutated alleles of mouse *TMEM16F* in *16F⁻/⁻*, *DKO* and *TKO* (A), *P2X7* in *P2X7⁻/⁻*, *DKO*, and *TKO* (B), *Eros* in *TKO* (C) are shown. Protospacer sequences are highlighted in light blue, protospacer-adjacent motifs (PAM) are underlined in red, and the cleavage sites are pointed by red arrowheads. Sequences deleted, mutated or inserted are shown in blue, green, or red, respectively. In right panel of (A), the cell lysates from the wild type (lane 1) or *TMEM16F⁻/⁻* cells (lane 2) were separated by SDS-PAGE, and analyzed by Western blotting with rabbit anti-TMEM16F Ab (11).

22

A <u>hEros</u>

	45	46	47	48	49	50	51	52	53	54	55 (aa)
	Leu	Gly	Trp	Lys	Leu	Phe	Tyr	Val	Thr	Gly	Cys

5' CTG GGC TGG AAG CTC TTC TAC GTC AC<u>A GGC</u> TGC   3' | WT |
                                         ▲   PAM

	45	46	47	48	49	50	51	52	53	54	105 (aa)
	Leu	Gly	Trp	Lys	Leu	Phe	Tyr	Val	His	Arg ----	Pro ***

5' CTG GGC TGG AAG CTC TTC TAC GTT CAC AGG----CCA TGA   3' | Eros⁻ᐟ⁻ |

B <u>hP2X7</u>

	47	48	49	50	51	52	53	54	55	56	57	58	59	60	61	62	63 (aa)
	Ser	Asp	Lys	Leu	Tyr	Gln	Arg	Lys	Glu	Pro	Val	Ile	Ser	Ser	Val	His	Thr

5' AGT GAC AAG CTG TA<u>C CAG</u> CGG AAA GAG CCT GTC ATC AGT TCT GTG CAC ACC   3' | WT |
                          PAM   ▲

	42	43	44	45	46	47	48	49	74 (aa)
	Cys	Phe	Ala	Leu	Val	Ser	Ala	His ----Leu	***

5' TGC TTT GCT CTG GTG AGT GCA CAC----CTT TGA   3' | P2X7⁻ᐟ⁻ |

Supplemental Figure 2. Gene knock-out in human THP-1 cells by CRISPR-Cas9 system.
The wild-type and mutated alleles of human *Eros* in *Eros⁻ᐟ⁻* THP-1 (A) and *P2X7* in *P2X7⁻ᐟ⁻* THP-1 cells (B) are shown. Protospacer sequences are highlighted in light blue, protospacer-adjacent motifs (PAM) are underlined in red, and the cleavage sites are pointed by red arrowheads. Sequences deleted, mutated or inserted are shown in blue, green, or red, respectively.

5. Discussion

TMEM16F mediates Ca^{2+}-induced PtdSer exposure in platelets, lymphocytes, and myoblasts (90, 91). Because the P2X7-mediated PtdSer exposure is accompanied by Ca^{2+} influx, TMEM16F was proposed to be involved in this process (68). However, I showed in this study that a TMEM16F-null mutation in mouse T cell lines had little effect on the P2X7-induced PtdSer exposure. Preliminary results in Nagata group also showed that TMEM16F-null BMDMs responded to BzATP to expose PtdSer as efficiently as wild-type macrophages to expose PtdSer. Although I cannot rule out the possibility that Ca^{2+} internalized by a P2X7-mediated ion channel activates TMEM16F to expose PtdSer, it is clear that a TMEM16F-independent mechanism also exists for the P2X7-mediated PtdSer exposure. Two families of membrane proteins (TMEM16F and XKR) have phospholipid scramblase activity (90). Treatment with an intracellular Ca^{2+} chelator did not inhibit the P2X7-induced PtdSer exposure, suggesting that TMEM16 family members are not involved in this process. Whether a member of the XKR family or another unidentified molecule is responsible for the P2X7-mediated PtdSer exposure remains to be studied.

Screening of the GeCKO-CRISPR library (71) identified Eros as the molecule essential for the high, stable expression of P2X7. Eros is a membrane protein carrying two transmembrane regions. Thomas et al. (89) previously showed that Eros is localized to the endoplasmic reticulum and functions as a chaperone for the components of NADPH oxidase, a heterodimeric complex of gp91^{phox} and p22^{phox}, present in the plasma membrane. Similarly, I found that Eros was located at the endoplasmic reticulum, in WR19L cells. BN-PAGE and immunoprecipitation analyses indicated that P2X7 was present in two forms: associated or not associated with Eros. The intracellular colocalization of P2X7 with Eros suggested that Eros binds to P2X7 at the endoplasmic reticulum and helps its folding. Once P2X7 is correctly folded, it leaves the endoplasmic reticulum and moves to the plasma membrane, whereas Eros is recycled to act as a chaperone for newly synthesized P2X7 molecules. The recycling of chaperones requires energy or ATP (92). Eros does not appear to carry an ATPase or nucleotide-binding domain, indicating that Eros may act as a cochaperone for specific client proteins (e.g., NADPH oxidase and P2X7). As is found for many other membrane proteins (93), other classical chaperones (Hsp90 and Hsp70) with ATPase activity may be involved in the folding of P2X7. In this regard, it may be relevant that the NADPH oxidase activity is regulated by Hsp90 (94).

Similar to mutations in NADPH oxidase, loss-of-function mutations in Eros cause chronic granulomatous disease in humans (95, 96). There are two antimicrobial systems in phagocytes: reactive oxygen species (ROS) in the early host response, and reactive nitrogen species (RNS) in the late or chronic phase of infection (97-99). Accordingly, mice lacking both NADPH oxidase and inducible NO synthase exhibit a much stronger immunocompromised phenotype, such as granuloma

formation, than mice lacking only one of these systems (100). NADPH oxidase is responsible for ROS generation, whereas RNS are generated by the action of inducible NO synthase, the expression of which is upregulated by signaling from P2X7 (101). These results suggest that Eros, acting as a chaperone for NADPH oxidase and P2X7, regulates the production of both ROS and RNS. It would be interesting to examine whether the RNS system is defective in Eros-null macrophages. Although the inflammasomes for IL-1β production are activated, not only by the P2X7 pathway, but also by other noncanonical pathways (102), P2X7 was shown to be necessary for the ATP-induced IL-1β production in LPS-treated mice (63). It will be interesting to examine whether Eros-null mice or patients produce IL-1β and, if so, to correlate its level with the formation of granuloma.

P2X7 mutants including a spliced form that lacks the C-terminal region, or a form that carries point mutations in the C-terminal region, maintain their ion channel activity but cannot mediate the pore formation or cell death (54, 103, 104), suggesting that these signaling pathways are independent of the Ca^{2+} internalization or that they require an additional signal from the C-terminal cytoplasmic region of the P2X7 receptor. Screening a CRISPR library for certain respective outcomes, such as YO-PRO-1 uptake, IL-1β release, or PtdCho uptake, may identify molecules responsible for their specific signaling pathways.

6. References

1. van Meer, G., D. R. Voelker, and G. W. Feigenson. 2008. Membrane lipids: where they are and how they behave. *Nat. Rev. Mol. Cell Biol.* 9: 112–124.

2. Bevers, E. M., and P. L. Williamson. 2016. Getting to the outer leaflet: physiology of phosphatidylserine exposure at the plasma membrane. *Physiol. Rev.* 96: 605–645.

3. Leventis, P. A., and S. Grinstein. 2010. The distribution and function of phosphatidylserine in cellular membranes. *Annu. Rev. Biophys.* 39: 407–427.

4. Segawa, K., S. Kurata, Y. Yanagihashi, T. R. Brummelkamp, F. Matsuda, and S. Nagata. 2014. Caspase-mediated cleavage of phospholipid flippase for apoptotic phosphatidylserine exposure. *Science* 344: 1164–1168.

5. Segawa, K., S. Kurata, and S. Nagata. 2016. Human type IV P-type ATPases that work as plasma membrane phospholipid flippases and their regulation by caspase and calcium. *J. Biol. Chem.* 291: 762–772.

6. Segawa, K., S. Kurata, and S. Nagata. 2018. The CDC50A extracellular domain is required for forming a functional complex with and chaperoning phospholipid flippases to the plasma membrane. *J Biol Chem* 293: 2172-2182.

7. Kornberg, R. D., and H. M. McConnell. 1971. Inside-outside transitions of phospholipids in

vesicle membranes. *Biochemistry* 10: 1111-1120.

8. Ganong, B. R., and R. M. Bell. 1984. Transmembrane movement of phosphatidylglycerol and diacylglycerol sulfhydryl analogues. *Biochemistry* 23: 4977-4983.

9. Suzuki, J., M. Umeda, P. J. Sims, and S. Nagata. 2010. Calcium-dependent phospholipid scrambling by TMEM16F. *Nature* 468: 834–838.

10. Suzuki, J., D. P. Denning, E. Imanishi, H. R. Horvitz, and S. Nagata. 2013. Xk-related protein 8 and CED-8 promote phosphatidylserine exposure in apoptotic cells. *Science* 341: 403–406.

11. Suzuki, J., T. Fujii, T. Imao, K. Ishihara, H. Kuba, and S. Nagata. 2013. Calcium dependent phospholipid scramblase activity of TMEM16 protein family members. *J. Biol. Chem.* 288: 13305–13316.

12. Suzuki, J., E. Imanishi, and S. Nagata. 2014. Exposure of phosphatidylserine by Xk-related protein family members during apoptosis. *J. Biol. Chem.* 289: 30257– 30267.

13. Suzuki, J., E. Imanishi, and S. Nagata. 2016. Xkr8 phospholipid scrambling complex in apoptotic phosphatidylserine exposure. *Proc. Natl. Acad. Sci. USA* 113: 9509–9514.

14. Nagata, S., R. Hanayama, and K. Kawane. 2010. Autoimmunity and the clearance of dead cells. *Cell* 140: 619-630.

15. Kawano, M., and S. Nagata. 2018. Lupus-like autoimmune disease caused by a lack of Xkr8, a caspase-dependent phospholipid scramblase. *Proc Natl Acad Sci U S A* 115: 2132-2137.

16. Fujii, T., A. Sakata, S. Nishimura, K. Eto, and S. Nagata. 2015. TMEM16F is required for phosphatidylserine exposure and microparticle release in activated mouse platelets. *Proc. Natl. Acad. Sci. USA* 112: 12800–12805.

17. Sims, P. J., T. Wiedmer, C. T. Esmon, H. J. Weiss, and S. J. Shattil. 1989. Assembly of the platelet prothrombinase complex is linked to vesiculation of the platelet plasma membrane. Studies in Scott syndrome: an isolated defect in platelet procoagulant activity. *J. Biol. Chem.* 264: 17049–17057.

18. Dachary-Prigent, J., J. M. Pasquet, J. M. Freyssinet, and A. T. Nurden. 1995. Calcium involvement in aminophospholipid exposure and microparticle formation during platelet activation: a study using Ca2+-ATPase inhibitors. *Biochemistry* 34: 11625-11634.

19. Marsault, R., M. Murgia, T. Pozzan, and R. Rizzuto. 1997. Domains of high Ca2+ beneath the plasma membrane of living A7r5 cells. *EMBO J* 16: 1575-1581.

20. Hussain, J. F., and M. P. Mahaut-Smith. 1999. Reversible and irreversible intracellular Ca2+ spiking in single isolated human platelets. *J Physiol* 514 (Pt 3): 713-718.

21. de Vries, K. J., T. Wiedmer, P. J. Sims, and B. M. Gadella. 2003. Caspase-independent exposure of aminophospholipids and tyrosine phosphorylation in bicarbonate responsive human sperm cells. *Biol Reprod* 68: 2122-2134.

22. Elliott, J. I., A. Surprenant, F. M. Marelli-Berg, J. C. Cooper, R. L. Cassady-Cain, C. Wooding,

K. Linton, D. R. Alexander, and C. F. Higgins. 2005. Membrane phosphatidylserine distribution as a non-apoptotic signalling mechanism in lymphocytes. *Nat Cell Biol* 7: 808-816.

23. Fischer, K., S. Voelkl, J. Berger, R. Andreesen, T. Pomorski, and A. Mackensen. 2006. Antigen recognition induces phosphatidylserine exposure on the cell surface of human CD8+ T cells. *Blood* 108: 4094-4101.

24. Elliott, J. I., A. Sardini, J. C. Cooper, D. R. Alexander, S. Davanture, G. Chimini, and C. F. Higgins. 2006. Phosphatidylserine exposure in B lymphocytes: a role for lipid packing. *Blood* 108: 1611-1617.

25. Martin, S., I. Pombo, P. Poncet, B. David, M. Arock, and U. Blank. 2000. Immunologic stimulation of mast cells leads to the reversible exposure of phosphatidylserine in the absence of apoptosis. *Int Arch Allergy Immunol* 123: 249-258.

26. Riedl, S., B. Rinner, M. Asslaber, H. Schaider, S. Walzer, A. Novak, K. Lohner, and D. Zweytick. 2011. In search of a novel target - phosphatidylserine exposed by non-apoptotic tumor cells and metastases of malignancies with poor treatment efficacy. *Biochim Biophys Acta* 1808: 2638-2645.

27. Courageot, M. P., S. Lepine, F. Giraud, and J. C. Sulpice. 2002. Extracellular ATP induces phosphatidylserine externalization earlier than nuclear apoptotic events in thymocytes. *Ann N Y Acad Sci* 973: 186-189.

28. Wang, J. C. 2002. Cellular roles of DNA topoisomerases: a molecular perspective. *Nat Rev Mol Cell Biol* 3: 430-440.

29. Singleton, M. R., M. S. Dillingham, and D. B. Wigley. 2007. Structure and mechanism of helicases and nucleic acid translocases. *Annu Rev Biochem* 76: 23-50.

30. Cusack, S. 1997. Aminoacyl-tRNA synthetases. *Curr Opin Struct Biol* 7: 881-889.

31. Gouaux, E., and R. Mackinnon. 2005. Principles of selective ion transport in channels and pumps. *Science* 310: 1461-1465.

32. Jorgensen, P. L., K. O. Hakansson, and S. J. Karlish. 2003. Structure and mechanism of Na,K-ATPase: functional sites and their interactions. *Annu Rev Physiol* 65: 817-849.

33. Lunt, S. Y., and M. G. Vander Heiden. 2011. Aerobic glycolysis: meeting the metabolic requirements of cell proliferation. *Annu Rev Cell Dev Biol* 27: 441-464.

34. Ullrich, A., and J. Schlessinger. 1990. Signal transduction by receptors with tyrosine kinase activity. *Cell* 61: 203-212.

35. Chang, L., and M. Karin. 2001. Mammalian MAP kinase signalling cascades. *Nature* 410: 37-40.

36. Pellegatti, P., L. Raffaghello, G. Bianchi, F. Piccardi, V. Pistoia, and F. Di Virgilio. 2008. Increased level of extracellular ATP at tumor sites: in vivo imaging with plasma membrane luciferase. *PLoS One* 3: e2599.

37. Wilhelm, K., J. Ganesan, T. Müller, C. Dürr, M. Grimm, A. Beilhack, C. D. Krempl, S. Sorichter, U. V. Gerlach, E. Jüttner, A. Zerweck, F. Gärtner, P. Pellegatti, F. Di Virgilio, D. Ferrari, N. Kambham, P. Fisch, J. Finke, M. Idzko, and R. Zeiser. 2010. Graft-versus-host disease is enhanced by extracellular ATP activating P2X7R. *Nat Med* 16: 1434-1438.

38. Barberà-Cremades, M., A. Baroja-Mazo, A. I. Gomez, F. Machado, F. Di Virgilio, and P. Pelegrín. 2012. P2X7 receptor-stimulation causes fever via PGE2 and IL-1β release. *FASEB J* 26: 2951-2962.

39. Linden, J., F. Koch-Nolte, and G. Dahl. 2019. Purine release, metabolism, and signaling in the inflammatory response. *Annu. Rev. Immunol.* 37: 325–347.

40. Verkhratsky, A., and G. Burnstock. 2014. Biology of purinergic signalling: its ancient evolutionary roots, its omnipresence and its multiple functional significance. *Bioessays* 36: 697-705.

41. von Kügelgen, I., and K. Hoffmann. 2016. Pharmacology and structure of P2Y receptors. *Neuropharmacology* 104: 50-61.

42. Cicko, S., M. Lucattelli, T. Müller, M. Lommatzsch, G. De Cunto, S. Cardini, W. Sundas, M. Grimm, R. Zeiser, T. Dürk, G. Zissel, J. M. Boeynaems, S. Sorichter, D. Ferrari, F. Di Virgilio, J. C. Virchow, G. Lungarella, and M. Idzko. 2010. Purinergic receptor inhibition prevents the development of smoke-induced lung injury and emphysema. *J Immunol* 185: 688-697.

43. Müller, T., B. Robaye, R. P. Vieira, D. Ferrari, M. Grimm, T. Jakob, S. F. Martin, F. Di Virgilio, J. M. Boeynaems, J. C. Virchow, and M. Idzko. 2010. The purinergic receptor P2Y2 receptor mediates chemotaxis of dendritic cells and eosinophils in allergic lung inflammation. *Allergy* 65: 1545-1553.

44. Müller, T., S. Fay, R. P. Vieira, H. Karmouty-Quintana, S. Cicko, K. Ayata, G. Zissel, T. Goldmann, G. Lungarella, D. Ferrari, F. Di Virgilio, B. Robaye, J. M. Boeynaems, M. R. Blackburn, and M. Idzko. 2017. The purinergic receptor subtype P2Y2 mediates chemotaxis of neutrophils and fibroblasts in fibrotic lung disease. *Oncotarget* 8: 35962-35972.

45. Wilkin, F., X. Duhant, C. Bruyns, N. Suarez-Huerta, J. M. Boeynaems, and B. Robaye. 2001. The P2Y11 receptor mediates the ATP-induced maturation of human monocyte-derived dendritic cells. *J Immunol* 166: 7172-7177.

46. Khakh, B. S., G. Burnstock, C. Kennedy, B. F. King, R. A. North, P. Séguéla, M. Voigt, and P. P. Humphrey. 2001. International union of pharmacology. XXIV. Current status of the nomenclature and properties of P2X receptors and their subunits. *Pharmacol Rev* 53: 107-118.

47. Kawate, T., J. C. Michel, W. T. Birdsong, and E. Gouaux. 2009. Crystal structure of the ATP-gated P2X(4) ion channel in the closed state. *Nature* 460: 592–598.

48. McCarthy, A. E., C. Yoshioka, and S. E. Mansoor. 2019. Full-Length P2X7 structures reveal how palmitoylation prevents channel desensitization. *Cell* 179: 659–670.e13.

49. Hattori, M., and E. Gouaux. 2012. Molecular mechanism of ATP binding and ion channel activation in P2X receptors. *Nature* 485: 207-212.

50. North, R. A. 2002. Molecular physiology of P2X receptors. *Physiol. Rev.* 82: 1013–1067.

51. Khakh, B. S., and R. A. North. 2012. Neuromodulation by extracellular ATP and P2X receptors in the CNS. *Neuron* 76: 51-69.

52. Bartlett, R., L. Stokes, and R. Sluyter. 2014. The P2X7 receptor channel: recent developments and the use of P2X7 antagonists in models of disease. *Pharmacol Rev* 66: 638-675.

53. Di Virgilio, F., D. Dal Ben, A. C. Sarti, A. L. Giuliani, and S. Falzoni. 2017. The P2X7 receptor in infection and inflammation. *Immunity* 47: 15–31.

54. Surprenant, A., F. Rassendren, E. Kawashima, R. A. North, and G. Buell. 1996. The cytolytic P2Z receptor for extracellular ATP identified as a P2X receptor (P2X7). *Science* 272: 735–738.

55. Mariathasan, S., D. S. Weiss, K. Newton, J. McBride, K. O'Rourke, M. Roose-Girma, W. P. Lee, Y. Weinrauch, D. M. Monack, and V. M. Dixit. 2006. Cryopyrin activates the inflammasome in response to toxins and ATP. *Nature* 440: 228–232.

56. Virginio, C., A. MacKenzie, R. A. North, and A. Surprenant. 1999. Kinetics of cell lysis, dye uptake and permeability changes in cells expressing the rat P2X7 receptor. *J Physiol* 519 Pt 2: 335-346.

57. Browne, L. E., V. Compan, L. Bragg, and R. A. North. 2013. P2X7 receptor channels allow direct permeation of nanometer-sized dyes. *J Neurosci* 33: 3557-3566.

58. Scheuplein, F., N. Schwarz, S. Adriouch, C. Krebs, P. Bannas, B. Rissiek, M. Seman, F. Haag, and F. Koch-Nolte. 2009. NAD+ and ATP released from injured cells induce P2X7-dependent shedding of CD62L and externalization of phosphatidylserine by murine T cells. *J. Immunol.* 182: 2898–2908.

59. MacKenzie, A., H. L. Wilson, E. Kiss-Toth, S. K. Dower, R. A. North, and A. Surprenant. 2001. Rapid secretion of interleukin-1beta by microvesicle shedding. *Immunity* 15: 825–835.

60. Mackenzie, A. B., M. T. Young, E. Adinolfi, and A. Surprenant. 2005. Pseudoapoptosis induced by brief activation of ATP-gated P2X7 receptors. *J Biol Chem* 280: 33968-33976.

61. Taylor, S. R., M. Gonzalez-Begne, S. Dewhurst, G. Chimini, C. F. Higgins, J. E. Melvin, and J. I. Elliott. 2008. Sequential shrinkage and swelling underlie P2X7-stimulated lymphocyte phosphatidylserine exposure and death. *J Immunol* 180: 300-308.

62. Barberà-Cremades, M., A. I. Gómez, A. Baroja-Mazo, L. Martínez-Alarcón, C. M. Martínez, C. de Torre-Minguela, and P. Pelegrín. 2017. P2X7 Receptor Induces Tumor Necrosis Factor-α Converting Enzyme Activation and Release to Boost TNF-α Production. *Front Immunol* 8: 862.

63. Solle, M., J. Labasi, D. G. Perregaux, E. Stam, N. Petrushova, B. H. Koller, R. J. Griffiths, and C. A. Gabel. 2001. Altered cytokine production in mice lacking P2X(7) receptors. *J. Biol. Chem.* 276: 125–132.

64. Miller, C. M., N. R. Boulter, S. J. Fuller, A. M. Zakrzewski, M. P. Lees, B. M. Saunders, J. S. Wiley, and N. C. Smith. 2011. The role of the P2X$_7$ receptor in infectious diseases. *PLoS Pathog* 7: e1002212.

65. Taylor, S. R., C. M. Turner, J. I. Elliott, J. McDaid, R. Hewitt, J. Smith, M. C. Pickering, D. L. Whitehouse, H. T. Cook, G. Burnstock, C. D. Pusey, R. J. Unwin, and F. W. Tam. 2009. P2X7 deficiency attenuates renal injury in experimental glomerulonephritis. *J Am Soc Nephrol* 20: 1275-1281.

66. Weber, F. C., P. R. Esser, T. Müller, J. Ganesan, P. Pellegatti, M. M. Simon, R. Zeiser, M. Idzko, T. Jakob, and S. F. Martin. 2010. Lack of the purinergic receptor P2X(7) results in resistance to contact hypersensitivity. *J Exp Med* 207: 2609-2619.

67. Martins, J. P., R. B. Silva, R. Coutinho-Silva, C. M. Takiya, A. M. Battastini, F. B. Morrone, and M. M. Campos. 2012. The role of P2X7 purinergic receptors in inflammatory and nociceptive changes accompanying cyclophosphamide-induced haemorrhagic cystitis in mice. *Br J Pharmacol* 165: 183-196.

68. Ousingsawat, J., P. Wanitchakool, A. Kmit, A. M. Romao, W. Jantarajit, R. Schreiber, and K. Kunzelmann. 2015. Anoctamin 6 mediates effects essential for innate immunity downstream of P2X7 receptors in macrophages. *Nat. Commun.* 6: 6245.

69. Mizushima, S., and S. Nagata. 1990. pEF-BOS, a powerful mammalian expression vector. *Nucleic Acids Res.* 18: 5322.

70. Ochi, A., R. G. Hawley, M. J. Shulman, and N. Hozumi. 1983. Transfer of a cloned immunoglobulin light-chain gene to mutant hybridoma cells restores specific antibody production. *Nature* 302: 340–342.

71. Sanjana, N. E., O. Shalem, and F. Zhang. 2014. Improved vectors and genome-wide libraries for CRISPR screening. *Nat. Methods* 11: 783–784.

72. Ran, F. A., P. D. Hsu, J. Wright, V. Agarwala, D. A. Scott, and F. Zhang. 2013. Genome engineering using the CRISPR-Cas9 system. *Nat. Protoc.* 8: 2281–2308.

73. Miyoshi, H., U. Blo¨mer, M. Takahashi, F. H. Gage, and I. M. Verma. 1998. Development of a self-inactivating lentivirus vector. *J. Virol.* 72: 8150–8157.

74. Kitamura, T., Y. Koshino, F. Shibata, T. Oki, H. Nakajima, T. Nosaka, and H. Kumagai. 2003. Retrovirus-mediated gene transfer and expression cloning: powerful tools in functional genomics. *Exp. Hematol.* 31: 1007–1014.

75. Morita, S., T. Kojima, and T. Kitamura. 2000. Plat-E: an efficient and stable system for transient packaging of retroviruses. *Gene Ther.* 7: 1063–1066.

76. Rassendren, F., G. N. Buell, C. Virginio, G. Collo, R. A. North, and A. Surprenant. 1997. The permeabilizing ATP receptor, P2X7. Cloning and expression of a human cDNA. *J. Biol. Chem.* 272: 5482–5486.

77. Nicke, A., Y.-H. Kuan, M. Masin, J. Rettinger, B. Marquez-Klaka, O. Bender, D. C. Go´recki, R. D. Murrell-Lagnado, and F. Soto. 2009. A functional P2X7 splice variant with an alternative transmembrane domain 1 escapes gene inactivation in P2X7 knock-out mice. *J. Biol. Chem.* 284: 25813–25822.

78. Shalem, O., N. E. Sanjana, E. Hartenian, X. Shi, D. A. Scott, T. Mikkelson, D. Heckl, B. L. Ebert, D. E. Root, J. G. Doench, and F. Zhang. 2014. Genomescale CRISPR-Cas9 knockout screening in human cells. *Science* 343: 84–87.

79. Joung, J., S. Konermann, J. S. Gootenberg, O. O. Abudayyeh, R. J. Platt, M. D. Brigham, N. E. Sanjana, and F. Zhang. 2017. Genome-scale CRISPR-Cas9 knockout and transcriptional activation screening. [Published erratum appears in 2019 *Nat. Protoc.* 14: 2259.] *Nat. Protoc.* 12: 828–863.

80. Daigneault, M., J. A. Preston, H. M. Marriott, M. K. B. Whyte, and D. H. Dockrell. 2010. The identification of markers of macrophage differentiation in PMA-stimulated THP-1 cells and monocyte-derived macrophages. *PLoS One* 5: e8668.

81. Takeshita, S., K. Kaji, and A. Kudo. 2000. Identification and characterization of the new osteoclast progenitor with macrophage phenotypes being able to differentiate into mature osteoclasts. *J. Bone Miner. Res.* 15: 1477–1488.

82. Di Virgilio, F., P. Chiozzi, D. Ferrari, S. Falzoni, J. M. Sanz, A. Morelli, M. Torboli, G. Bolognesi, and O. R. Baricordi. 2001. Nucleotide receptors: an emerging family of regulatory molecules in blood cells. *Blood* 97: 587–600.

83. Cheewatrakoolpong, B., H. Gilchrest, J. C. Anthes, and S. Greenfeder. 2005. Identification and characterization of splice variants of the human P2X7 ATP channel. *Biochem. Biophys. Res. Commun.* 332: 17–27.

84. Xu, X. J., M. Boumechache, L. E. Robinson, V. Marschall, D. C. Gorecki, M. Masin, and R. D. Murrell-Lagnado. 2012. Splice variants of the P2X7 receptor reveal differential agonist dependence and functional coupling with pannexin-1. *J. Cell Sci.* 125: 3776–3789.

85. Courageot, M.-P., S. Le´pine, M. Hours, F. Giraud, and J.-C. Sulpice. 2004. Involvement of sodium in early phosphatidylserine exposure and phospholipid scrambling induced by P2X7 purinoceptor activation in thymocytes. *J. Biol. Chem.* 279: 21815–21823.

86. Virginio, C., A. MacKenzie, R. A. North, and A. Surprenant. 1999. Kinetics of cell lysis, dye uptake and permeability changes in cells expressing the rat P2X7 receptor. *J. Physiol.* 519: 335–346.

87. Humphreys, B. D., and G. R. Dubyak. 1996. Induction of the P2z/P2X7 nucleotide receptor and associated phospholipase D activity by lipopolysaccharide and IFN-gamma in the human THP-1 monocytic cell line. *J. Immunol.* 157: 5627–5637.

88. Ferrari, D., P. Chiozzi, S. Falzoni, M. Dal Susino, L. Melchiorri, O. R. Baricordi, and F. Di

Virgilio. 1997. Extracellular ATP triggers IL-1 beta release by activating the purinergic P2Z receptor of human macrophages. *J. Immunol.* 159: 1451–1458.

89. Thomas, D. C., S. Clare, J. M. Sowerby, M. Pardo, J. K. Juss, D. A. Goulding, L. van der Weyden, D. Storisteanu, A. Prakash, M. Espe´li, et al. 2017. Eros is a novel transmembrane protein that controls the phagocyte respiratory burst and is essential for innate immunity. *J. Exp. Med.* 214: 1111–1128.

90. Nagata, S., J. Suzuki, K. Segawa, and T. Fujii. 2016. Exposure of phosphatidylserine on the cell surface. *Cell Death Differ.* 23: 952–961.

91. Falzone, M. E., M. Malvezzi, B.-C. Lee, and A. Accardi. 2018. Known structures and unknown mechanisms of TMEM16 scramblases and channels. *J. Gen. Physiol.* 150: 933–947.

92. Genest, O., S. Wickner, and S. M. Doyle. 2019. Hsp90 and Hsp70 chaperones: collaborators in protein remodeling. *J. Biol. Chem.* 294: 2109–2120.

93. Yang, Y., B. Liu, J. Dai, P. K. Srivastava, D. J. Zammit, L. Lefranc¸ois, and Z. Li. 2007. Heat shock protein gp96 is a master chaperone for toll-like receptors and is important in the innate function of macrophages. *Immunity* 26: 215–226.

94. Chen, F., D. Pandey, A. Chadli, J. D. Catravas, T. Chen, and D. J. R. Fulton. 2011. Hsp90 regulates NADPH oxidase activity and is necessary for superoxide but not hydrogen peroxide production. Antioxid. *Redox Signal.* 14: 2107–2119.

95. Thomas, D. C., L.-M. Charbonnier, A. Schejtman, H. Aldhekri, E. L. Coomber, E. R. Dufficy, A. E. Beenken, J. C. Lee, S. Clare, A. O. Speak, et al. 2019. EROS/CYBC1 mutations: decreased NADPH oxidase function and chronic granulomatous disease. *J. Allergy Clin. Immunol.* 143: 782–785.e1.

96. Arnadottir, G. A., G. L. Norddahl, S. Gudmundsdottir, A. B. Agustsdottir, S. Sigurdsson, B. O. Jensson, K. Bjarnadottir, F. Theodors, S. Benonisdottir, E. V. Ivarsdottir, et al. 2018. A homozygous loss-of-function mutation leading to CYBC1 deficiency causes chronic granulomatous disease. *Nat. Commun.* 9: 4447.

97. Fang, F. C. 2004. Antimicrobial reactive oxygen and nitrogen species: concepts and controversies. *Nat. Rev. Microbiol.* 2: 820–832.

98. Mastroeni, P., A. Vazquez-Torres, F. C. Fang, Y. Xu, S. Khan, C. E. Hormaeche, and G. Dougan. 2000. Antimicrobial actions of the NADPH phagocyte oxidase and inducible nitric oxide synthase in experimental salmonellosis. II. Effects on microbial proliferation and host survival in vivo. *J. Exp. Med.* 192: 237–248.

99. Vazquez-Torres, A., J. Jones-Carson, P. Mastroeni, H. Ischiropoulos, and F. C. Fang. 2000. Antimicrobial actions of the NADPH phagocyte oxidase and inducible nitric oxide synthase in experimental salmonellosis. I. Effects on microbial killing by activated peritoneal macrophages in vitro. *J. Exp. Med.* 192: 227–236.

100. Shiloh, M. U., J. D. MacMicking, S. Nicholson, J. E. Brause, S. Potter, M. Marino, F. Fang, M. Dinauer, and C. Nathan. 1999. Phenotype of mice and macrophages deficient in both phagocyte oxidase and inducible nitric oxide synthase. *Immunity* 10: 29–38.

101. Guerra, A. N., P. L. Fisette, Z. A. Pfeiffer, B. H. Quinchia-Rios, U. Prabhu, M. Aga, L. C. Denlinger, A. G. Guadarrama, S. Abozeid, J. A. Sommer, et al. 2003. Purinergic receptor regulation of LPS-induced signaling and pathophysiology. *J. Endotoxin Res.* 9: 256–263.

102. Broz, P., and V. M. Dixit. 2016. Inflammasomes: mechanism of assembly, regulation and signalling. *Nat. Rev. Immunol.* 16: 407–420.

103. Feng, Y.-H., X. Li, L. Wang, L. Zhou, and G. I. Gorodeski. 2006. A truncated P2X7 receptor variant (P2X7-j) endogenously expressed in cervical cancer cells antagonizes the full-length P2X7 receptor through hetero-oligomerization. *J. Biol. Chem.* 281: 17228–17237.

104. Gu, B. J., W. Zhang, R. A. Worthington, R. Sluyter, P. Dao-Ung, S. Petrou, J. A. Barden, and J. S. Wiley. 2001. A Glu-496 to Ala polymorphism leads to loss of function of the human P2X7 receptor. *J. Biol. Chem.* 276: 11135– 11142.

7. Publication list

2. Asano, L., M. Watanabe, Y. Ryoden, K. Usuda, T. Yamaguchi, B. Khambu, M. Takashima, SI. Sato, J. Sakai, K. Nagasawa, M. Uesugi. 2017. Vitamin D Metabolite, 25-Hydroxyvitamin D, Regulates Lipid Metabolism by Inducing Degradation of SREBP/SCAP. Cell Chem. Biol. 24(2):207-217.

1. Ryoden, Y., T. Fujii, K. Segawa, S. Nagata. 2020. Functional Expression of the P2X7 ATP Receptor Requires Eros. J. Immunol. in press.

8. Acknowledgement